applied sciences

MDPI

Review

Application of Spinel and Hexagonal Ferrites in Heterogeneous Photocatalysis

Zuzanna Bielan [1,*], Szymon Dudziak [2], Adam Kubiak [3] and Ewa Kowalska [4,*]

[1] Centre for Plasma and Laser Engineering, The Szewalski Institute of Fluid-Flow Machinery, Polish Academy of Science, Fiszera 14, 80-231 Gdansk, Poland
[2] Department of Process Engineering and Chemical Technology, Chemical Faculty, Gdansk University of Technology, G. Narutowicza 11/12, 80-233 Gdansk, Poland; dudziakszy@gmail.com
[3] Institute of Chemistry and Technical Electrochemistry, Faculty of Chemical Technology, Poznan University of Technology, Berdychowo 4, 60-965 Poznan, Poland; adam.kubiak@put.poznan.pl
[4] Institute for Catalysis (ICAT), Hokkaido University, N21 W10, Sapporo 001-0021, Japan
* Correspondence: zbielan@imp.gda.pl (Z.B.); kowalska@cat.hokudai.ac.jp (E.K.)

Abstract: Semiconducting materials display unique features that enable their use in a variety of applications, including self-cleaning surfaces, water purification systems, hydrogen generation, solar energy conversion, etc. However, one of the major issues is separation of the used materials from the process suspension. Therefore, chemical compounds with magnetic properties have been proposed as crucial components of photocatalytic composites, facilitating separation and recovery of photocatalysts under magnetic field conditions. This review paper presents the current state of knowledge on the application of spinel and hexagonal ferrites in heterogeneous photocatalysis. The first part focuses on the characterization of magnetic (nano)particles. The next section presents the literature findings on the single-phase magnetic photocatalyst. Finally, the current state of scientific knowledge on the wide variety of magnetic-photocatalytic composites is presented. A key aim of this review is to indicate that spinel and hexagonal ferrites are considered as an important element of heterogeneous photocatalytic systems and are responsible for the effective recycling of the photocatalytic materials.

Keywords: heterogeneous photocatalysis; hexagonal ferrites; magnetic separation; spinel ferrites

Citation: Bielan, Z.; Dudziak, S.; Kubiak, A.; Kowalska, E. Application of Spinel and Hexagonal Ferrites in Heterogeneous Photocatalysis. *Appl. Sci.* **2021**, *11*, 10160. https://doi.org/10.3390/app112110160

Academic Editors: Francesco Congiu and Giorgio Concas

Received: 30 September 2021
Accepted: 26 October 2021
Published: 29 October 2021

1. Introduction

Nowadays, increasing global pollution and energy issues constitute the main threats to the natural environment. Therefore, new strategies and approaches have been developed to solve those issues. Among them, materials science might be considered as one of the crucial fields for environmental protection [1]. For example, oxide systems, defined as a material consisting of at least two components (oxides) aimed at improving the application properties of the final product, are becoming more and more popular. The growth of the application potential of oxide systems is due to the synergistic effects between components (e.g., heterojunction, Z-scheme mechanism, etc. [2]) or the formation of mixed crystallographic structures (e.g., $ZnTiO_3$, $SrTiO_3$ [3]). It should be emphasized, however, that apart from the chemical composition, the control of crystallite/particle sizes, in particular at the nano scale, is fundamental for further applications of oxide materials in photoactive processes (photocatalytic, photovoltaic, etc.) [4]. For this reason, the classic approach to materials' synthesis, where the size of the particles is not the main concern for the process efficiency, is currently one of the crucial issues in modern materials science.

Since the famous publication by Fujishima and Honda in 1972 [5], photocatalysis study using semiconductor materials has received increasing attention [6–9]. Each year, scientists from around the world are developing new photoactive materials, as well as modifying the known ones, in order to overcome their limitations with mass transfer, charge carrier

recombination, visible-light activity, separation, generation of reactive oxygen species, and effective irradiation [10–15].

Comparing the number of recently published manuscripts in the field of photocatalysis (Figure 1), only about 7% consider the material separation after the reaction, which is considerably less than those focusing on activity increase (84%) and visible-light response (80%). This clearly shows that the recycling and reuse of photocatalysts is still undervalued. Furthermore, it should be mentioned that the study of magnetic separation began relatively late (around beginning of the 21st century) in comparison to the other aspects of heterogeneous photocatalysis.

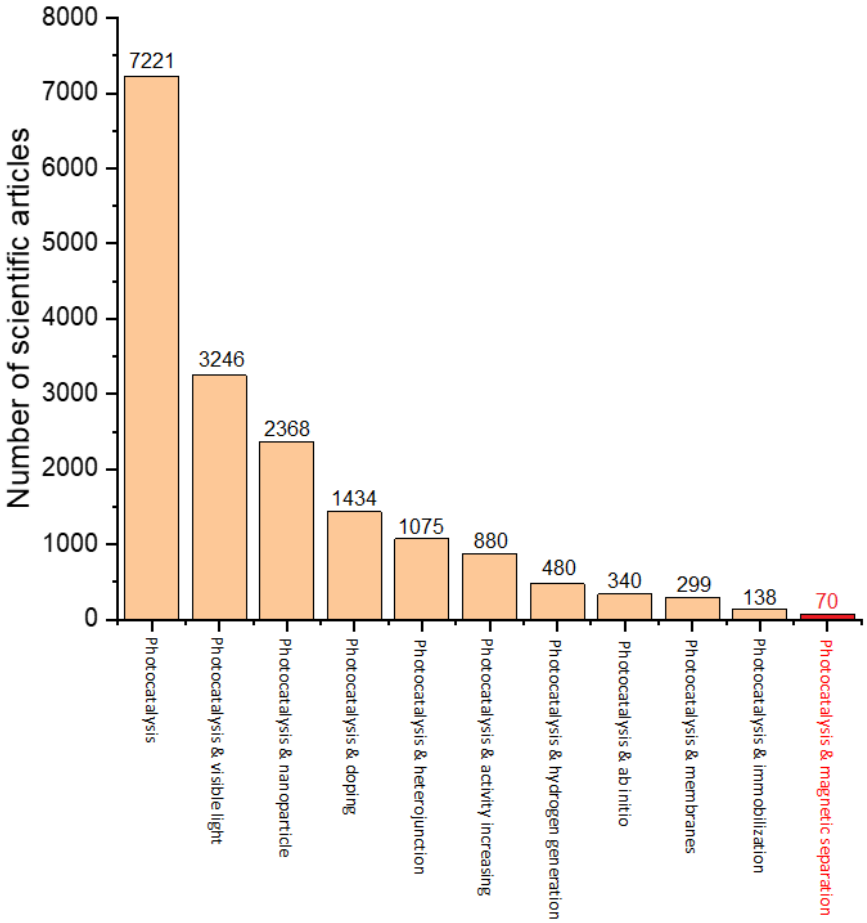

Figure 1. The number of scientific articles published in 2020 (according to the Web of Science database) for various keywords concerning photocatalysis.

Of course, other types of separation/recycling have been proposed and investigated, such as sedimentation, coagulation, (ultra)filtration, immobilization of photocatalysts on elements of photoreactors (walls [16], quartz protecting tubes of lamps and LEDs [17,18], and optical fibers [19]) or additional supporters (glass beads [16], microspheres [20], balls [21], mesh [22], cloth [22], rings [23], membranes [24–26], and plates/films/foils [27–30]) [31].

The main limitation of simple separation by gravitational sedimentation is caused by the nanometric size of photocatalysts. Kagaya et al. [32] as well as Baran et al. [33] proposed photocatalyst separation by coagulation. The addition of inorganic ($FeCl_3$ [33], $[Al_2(OH)_nCl_{6-n}]_m$ [32] and poly-ferric sulfate (PFS) [34]) or organic coagulants (e.g., cationic polyacrylamide (CPAM) [35]) might effectively accelerate the aggregation of photocatalyst nanoparticles (NPs) by modifying their double layer potential. Another method of suspended photocatalyst recovery is ultrafiltration. For example, Xue et al. [36] separated fine titania NPs by both cross-flow ultrafiltration (CFU) and coagulation. It has been found that

titania loses activity during coagulation, in contrast to CFU, which does not cause activity loss. However, the application of ultrafiltration is associated with significantly higher operation costs. In this respect, the immobilization of photocatalysts seems to be a better option. However, it is obvious that worse photocatalytic activity is expected for immobilized than suspended photocatalysts due to (i) mass transfer limitations, (ii) surface area decrease, and (iii) lower number of active sites for photocatalytic reactions. Additionally, the stability of immobilized photocatalysts is challenging, since photocatalyst leakage (detachment from the support [22,24,27]) and the destruction of suspended supports (e.g., microsphere breaking under shear forces inside the photoreactor [31]) have been observed. Accordingly, two different synthesis approaches have been proposed for efficient photocatalyst recovery: (i) mesoporous photocatalysts of micrometer size, thus allowing efficient separation by simple physical methods, i.e., sedimentation or filtration [37–39], and (ii) photocatalysts with magnetic properties. The latter is presented and discussed in this review.

The application of an external magnetic field, proposed as an alternative method of photocatalyst recovery, means that separated material must be bifunctional, i.e., with photocatalytic and magnetic properties. Ferromagnets have been viewed as the most promising magnetic materials to be used for this purpose. Their various combinations with popular semiconductors have been proposed in different configurations, i.e., from disordered mixtures [40], through more complex structures, such as core-shells [41], to advanced multilayered materials [42]. It should be pointed out that ferromagnet-semiconductor composites could also form efficient heterojunctions, since several magnetic oxides exhibit photocatalytic activity themselves [43], and thus the heterojunction composite might be even more active than the sole photocatalyst forming it. However, this might also result in the instability of the composite, as ferrites are not as photostable as typical photocatalysts (mainly titania), and thus dissolution and leakage of active components could occur due to photocorrosion. Accordingly, an insulator interlayer between the photocatalyst and ferrites has been proposed in more advanced structures.

In addition to the above-mentioned issues in the field of photocatalysis, attention should be paid to the fact that scientific knowledge in the subject of ab initio is still insufficient, as pointed out by, among others, Lisovski et al. [44]. Ab initio is a computational chemistry method based on quantum chemistry, and in the case of a photocatalyst, it enables determination of, among others, exciton lifetimes, stability, the redox position of valence and conduction bands, bandgap, and adsorption energies. For example, Hu et al. [45] explained the correlation between the packing factor and photocatalytic activity, whereas Lin et al. [46] successfully investigated the geometric structures and electronic properties of Ni-doped TiO_2 anatase and rutile. The authors described the calculation and simulation by a plane wave pseudopotential method based on density functional theory (DFT). However, the ab initio calculations in the field of photocatalysis are still challenging due to the current problems in computational chemistry; the vast majority of advanced experimental systems cannot be recreated, even by the supercomputer systems [47]. Therefore, it is necessary to further develop this field with regard to photooxidation processes [48] as well as the aspects of the separation of photocatalysts after processing.

This review presents all the aspects, focusing on the newest trends, applied for the use of spinel and hexagonal ferrites (selected groups of ferromagnets) in heterogeneous photocatalysis, as an efficient method for semiconductor recycling.

2. Characterization of Spinel and Hexagonal Ferrite Magnetic Nanoparticles

Ferrites, composite metal oxides containing ferric ions, are magnetic materials that have recently been intensively investigated for various possible applications, including electronic devices [49], gas sensors [50], medical purposes [51,52], water purification and wastewater treatment (adsorbent, catalyst, and Fenton reagent) [53–57], organic reactions (catalysts) [58,59], and heterogeneous photocatalysis [43]. Ferrites adopt mainly the spinel structure, but some exist in hexagonal one. The significant scientific interest in spinel and hexagonal ferrites is likely due to both their properties (magnetic properties, large specific

surface area) and simple and cheap synthesis procedure. Recently, they have also been applied for photocatalytic purposes, as discussed in the next sections.

2.1. Spinel Ferrites

Spinel ferrites with the general chemical formula of MFe_2O_4, where M states for metallic cation of Fe, Mg, Mn, Co, Zn, Ni, etc., are characterized by a cubic shape crystal structure, as presented in Figure 2. The distribution of M^{2+} and Fe^{3+} in the crystallographic sites (tetrahedral and octahedral) depends mainly on the M-cation radius and its charge, which obviously influence the final material properties [60,61]. In the case of normal spinel structures, M^{2+} cations occupy only tetrahedral sides, leaving octahedral ones for Fe^{3+}. Zinc ferrite ($ZnFe_2O_4$) is an example of this. In contrast, M^{2+} cations could also occupy only octahedral sides, forcing the partial migration of Fe^{3+} ions into the tetrahedra position, which is known as the inverse spinel structure (Fe_3O_4, $CoFe_2O_4$, $NiFe_2O_4$, etc.) [62].

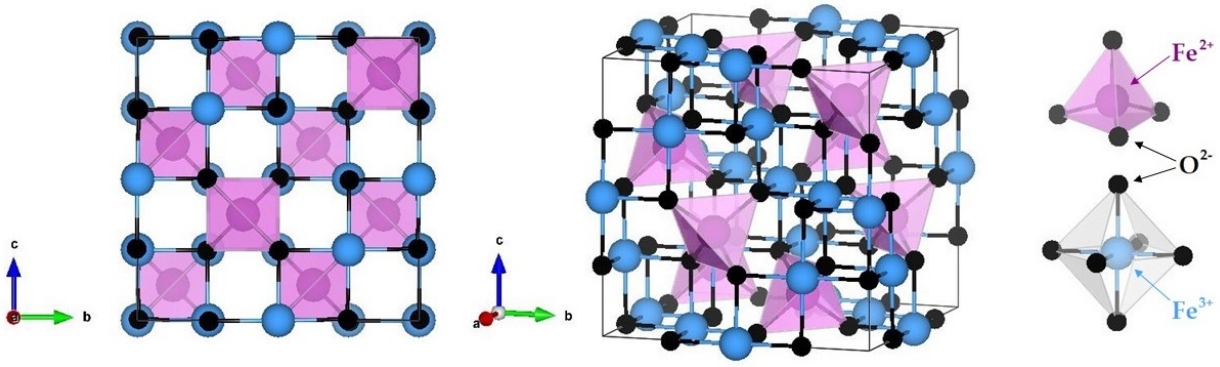

Figure 2. Spinel ferrite structure (inverse) for Fe_3O_4, presented along the a direction and as a 3D projection (not marked octahedra for clarity). Reprinted with permission from [63]. Copyright (2021) Creative Commons Attribution.

Magnetic properties of spinel ferrites strongly depend on their dimensions, i.e., the bigger the NP is, the higher is the value of magnetization saturation (M_s). Furthermore, superparamagnetism appears as a consequence of a decrease in ferromagnetic particle size to the nanometric scale. Usually, this occurs in NPs of the order of several nanometers to several dozens of nanometers, but the critical particle size is different for each material and is conditioned by magnetic anisotropy as well as chemical composition, crystal structure, and morphology of the ferrite [64]. As an example, magnetite NPs become superparamagnetites when their diameter is about 10–12 nm [65]. It should be pointed out that NPs lose their magnetization when the magnetic field is turned off.

2.2. Hexagonal Ferrites

Hexagonal ferrites (also referred as hexaferrites) represent a large class of magnetic ceramics with a hexagonal structure, which could be seen as an Fe_2O_3 network distorted by the presence of larger cations, usually Sr, Ba, or Pb. Compared to their spinel relatives, they generally (i) require higher temperatures to be synthesized, (ii) form larger particles easily, and (iii) exhibit typical hard-ferromagnetic behavior, with a large value of magnetic remanence and coercivity [66]. The hexaferrite family might be classified into six sub-categories, depending on the complexity of their crystal structure: M-type, Z-type, Y-type, W-type, X-type, and U-type ferrites [67]. However, regarding their photocatalytic applications, only M-type materials, with the general formula of $MFe_{12}O_{19}$, have been studied so far. Their crystal structure, using barium hexagonal ferrite ($BaFe_{12}O_{19}$) as an example, is presented in Figure 3.

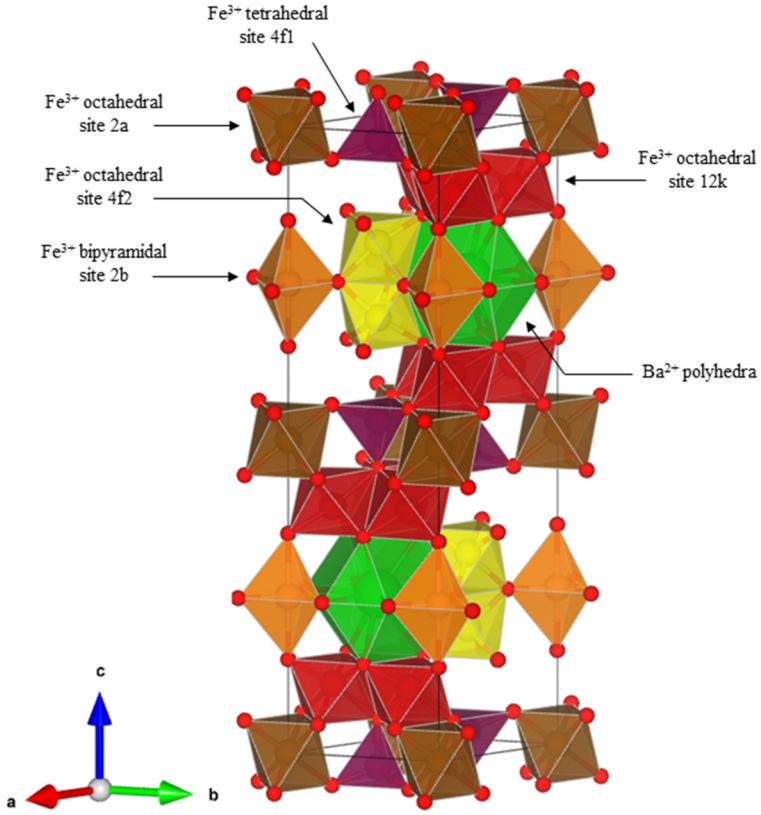

Figure 3. Crystal structure of the $BaFe_{12}O_{19}$ hexagonal ferrite.

3. Single-Phase Magnetic Photocatalysts

3.1. Spinel Ferrites

As presented by Zielińska-Jurek et al., pristine Fe_3O_4 (Eg = 0.1 eV) does not show any photocatalytic activity [68]. Nevertheless, some of MFe_2O_4 spinel ferrites are photocatalytically active themselves, without any coupling with other semiconductors (see Table 1). For example, Sutka et al. compared five different ferrites in terms of magnetic and photocatalytic properties [69]. It was found that materials with no or low M_s exhibit good photocatalytic activity for degradation of methyl orange (MO). Similarly, Dojcinovic et al. observed that with an increase in the content of doped cobalt in $Co_xMg_{1-x}Fe_2O_4$ ferrite, the magnetic properties increased, but photocatalytic activity decreased [70]. However, it has also been reported that manganese spinel ferrite ($MnFe_2O_4$) with a high M_s value (~60 $Am^2 \cdot kg^{-1}$) shows high photocatalytic activity (about 56% degradation of Direct Red 81 after 2 h of solar-light irradiation) [71]. It is also worth mentioning that the photocatalytic activity of spinel ferrites seems not to depend on their bandgap energies or on the conduction band (CB) and valence band (VB) positions, as they are similar for a wide range of materials (Figure 4).

Table 1. Summary of photocatalytic activity on spinel ferrites.

Photocatalyst	Pollutants	Experimental Conditions	Findings	Ref.
$MnFe_2O_4$	Direct Red 81	Solar light (Indonesia); 0.035 g·L^{-1}; 15–35 ppm; 120 min	56% deg. (15 ppm)	[71]
$MnFe_2O_4$	MB	500-W Hg lamp; 2–8 g·L^{-1}; 50 ppm; pH = 2–10; 5–35 min	~70% (35 min, 6 g·L^{-1}, pH 8.5)	[73]
MFe_2O_4 (M = Zn, Ni, Mg, Cu, Co)	MO	100-W LED; 1 g·L-1; 10 ppm; 180 min	$NiFe_2O_4$ 70% deg. $MgFe_2O_4$ ~30% deg. $ZnFe_2O_4$ ~15% deg. $CoFe_2O_4$ ~0 deg. $CuFe_2O_4$ ~0 deg.	[69]
$ZnSm_xFe_{2-x}O_4$ (x = 0–2)	MO	Solar light (India); 1 g·L^{-1}; 10–30 ppm; 80 min	$ZnSm_{1.5}Fe_{0.5}O_4$ 100% deg. (10 ppm); no activity loss after 5 runs	[74]
$Co_xMg_{1-x}Fe_2O_4$ (x = 0–1)	MB	Vis halogen lamp (70 mW·cm^{-2}) or natural sunlight (800–1100 W·m^{-2}); 0.5 g·L^{-1}; 10 ppm; 240 min	$Co_{0.1}Mg_{0.9}Fe_2O_4$ ~80% deg.	[70]
$Mg_{1-x}Ni_xFe_2O_4$ (x = 0.0, 0.6, 1.0)	MB	HEBER multilamp reactor; 0.1 g; 100 ppm; 2 ml Fenton's agent; 180 min	~86% deg.; negligible activity loss after 5 runs	[75]
Cu-$MgFe_2O_4$	MB	UV-lamp; 1 g·L^{-1}; 25 ppm; 180 min; 2 ml of H_2O_2	97% deg.; ca. 10% activity loss after 5 runs	[76]
$La_{1-x}Bi_xCr_{1-y}Fe_yO_3$ (x = 0–0.1; y = 0.02–0.12)	RhB	200 W Ar lamp/420 nm cut-off filter; 5 g·L^{-1}; 5 ml of 10% H_2O_2; 55 min	90.8% deg. ($La_{0.06}Bi_{0.04}Fe_{0.06}Cr_{0.08}O_3$)	[77]

deg.—degradation; MB—Methylene Blue; MO—Methyl Orange; RhB—Rhodamine B.

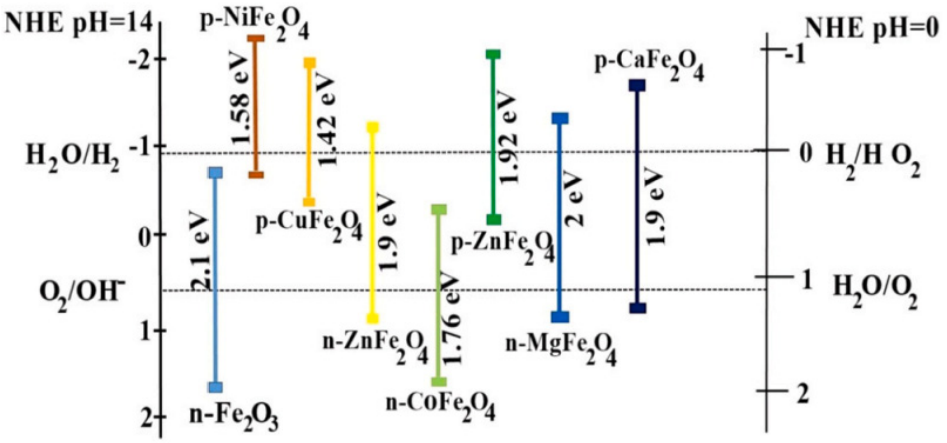

Figure 4. Bandgap energies of spinel ferrites (NHE, pH = 0 and 14). Reprinted with permission from [72]. Copyright (2021) Elsevier.

3.2. M-Type Hexaferrites

Concerning the photocatalytic activity of single-phase M-type hexaferrites, their efficiency is often much lower than that of known photocatalytic materials, but they can absorb a broad spectrum of visible light, and thus their vis activity is of some interest, as summarized in Table 2. For example, Bibi et al. studied the photocatalytic properties of pure and Nd/Cu co-doped $BaFe_{12}O_{19}$ under solar light in Pakistan, using methylene green dye as a probe [78]. Both types of ferrites could remove the target compound, with a final efficiency of 37% and 93% for pristine and doped materials, respectively, after 60 min of

irradiation. It has been proposed that the increased activity of a doped structure is caused by the possible formation of oxygen vacancies (due to the dopants' presence), which results in hindering of electron-hole recombination. Moreover, only a slight decrease in the efficiency from 93% to 91% was observed during five cycles, indicating high reusability of the Nd/Cu co-doped photocatalyst. Interestingly, Raut et al. showed that pristine $BaFe_{12}O_{19}$, prepared via the molten salt method, exhibits even higher photocatalytic activity than the well-known P25 TiO_2 (famous due to exceptionally high activity for various reactions and thus used as a standard for activity checking [79,80]) under both UV and UV/vis irradiation for degradation of hexahydro-1,3,5-trinitro-1,3,5-triazine (hexogen, RDX) [81]. The highest activity of the ferrite, observed under neutral pH conditions, was explained by efficient light absorption (bandgap of 2.1 eV) and thus an increased number of generated charge carriers. The high reusability of the photocatalyst was confirmed during three cycles, with the efficiency change from 100% to 98%. Bavarsiha et al. investigated the $SrFe_{12}O_{19}$ structure for photocatalytic degradation of methylene blue (MB) under UV irradiation [82]. It was found that 46% of dye could be removed during 120 min of irradiation, but reusability was not determined. Finally, the unique structure of the $CdFe_{12}O_{19}$ photocatalyst, both in its non-modified form (with some Fe_2O_3 impurities) and as a composite with $CdTiO_3$ phase, was investigated by Mahdiani et al. for removal of MB, methyl orange (MO), and methyl violet (MV) dyes under UV irradiation (without recycling analysis) [83]. It was found that the composite ($CdFe_{12}O_{19}/CdTiO_3$) is more active than a one-component photocatalyst for all the studied dyes, reaching the highest activity for MO—71% degradation during 70 min of irradiation.

Table 2. Summary of M-type hexaferrite photocatalysts.

Photocatalyst	Pollutants	Experimental Conditions	Findings	Ref.
$BaFe_{12}O_{19}$	MG	Pakistan sunlight; 882–890 $W \cdot m^{-2}$; 0.05 $g \cdot L^{-1}$; 10 ppm; 60 min	37% deg.	[78]
$BaFe_{12}O_{19}$ doped with Nb and Cu			93% deg.	
$BaFe_{12}O_{19}$	RXD	250 W Hg lamp (λ_{max} 254 nm); 300 W Hal. lamp (350–1100 nm); pH 3–10; 0.2–1.4 $g \cdot L^{-1}$; 40 ppm; 240 min	100% deg. (Hg lamp); 90% deg. (Hal. lamp)	[81]
$SrFe_{12}O_{19}$	MB	20 W UV light; 50 ppm; 120 min	46% deg.	[82]
$CdFe_{12}O_{19}$ (with Fe_2O_3 impurity)	MO; MB; MV	400 W UV light; 1 $g \cdot L^{-1}$; 5 ppm; 70 min	19% deg. MO; 0% deg. MB; 0 deg. MV	[83]
$CdFe_{12}O_{19}/CdTiO_3$			70% deg. MO; 61% deg. MB; 55% deg. MV	
$Ba_{1-x}Co_xFe_{12-y}Cr_yO_{19}$ (x = 0–0.7; y = 0–0.6)	CV	Bahawalpur (Pakistan) sunlight (881–892 $W \cdot m^{-2}$); 1 $g \cdot L^{-1}$; 10 ppm; 60 min	~65.5% deg.	[84]

CV—Crystal Violet dye; deg.—degradation; Hal.—halogen; MB—Methylene Blue; MG—Methyl Green; MO—Methyl Orange; MV—Methyl Violet; RXD—hexogen

4. TiO_2-Based Magnetic Photocatalysts

Titanium(IV) oxide (TiO_2, titania, titanium dioxide) is probably the most broadly investigated semiconductor photocatalyst due to various advantages, including high photocatalytic activity, stability, abundance, low price, and low toxicity [85–89]. However, the wide bandgap of titania, resulting in good redox properties (both oxidation and water reduction capabilities) is not recommended for light harvesting efficiency. Moreover, titania, as all semiconductors, suffers from charge carriers' recombination. In addition, the most active titania, i.e., that used in a particulate form, cannot be easily recycled, as already discussed in the introduction. Accordingly, various methods of titania modification, doping, coupling, and immobilizing have been proposed to improve its photocatalytic performance [14,90–94]. Ferrites have also been proposed as titania modifiers for three

main purposes, i.e., (i) improved activity by hindering the charge carriers' recombination, (ii) extension of activity towards vis range of solar spectrum, and (iii) easy and cheap recycling, as presented in this Section.

4.1. Spinel Ferrites with TiO_2

The coupling of spinel ferrites and titania (pristine or modified) in order to obtain a highly photoactive material with magnetic properties has commonly been reported in the recent literature, as summarized in Table 3.

Table 3. Summary of TiO_2-spinel ferrite photocatalysts.

Photocatalyst	Pollutants	Experimental Conditions	Findings	Ref.
Fe_3O_4@SiO_2/TiO_2-M (M = Pt/Cu)	Ph, 4-NPh	300 W Xe light (UV/vis, 60 W·m^{-2}); 2 g·L^{-1}; 20 ppm (Ph) or 500 µM (4 NPh); 60 min	10% 4-NPh deg. (Fe_3O_4@SiO_2/TiO_2); 100% Ph deg. and 50% TOC removal (Fe_3O_4@SiO_2/TiO_2-Pt)	[95]
$ZnFe_2O_4$/SiO_2/TiO_2	ETD	300 W Xe light (UV/vis or vis λ > 400 nm); 2 g·L^{-1}; 15 ppm; 30 min	100% deg. (UV/vis); 40% deg. (vis); 6 cycles	[96]
TiO_2-Fe_3O_4-M (M = Ag/Au)	Phenols	120 W Hg lamp (UV) or 150 W Hal. lamp (UV/vis, 350–700 nm); 2 g·L^{-1}; 1 mM; 7 h	~0.29 mm·h^{-1} (TiO_2-Fe_3O_4/Ag; UV); ~0.13 mm·h^{-1} (TiO_2-Fe_3O_4/Ag; vis)	[97]
$NiFe_2O_4$@TiO_2 core@shell	MO	300 W Xe lamp with cut-off filter (λ > 400 nm); 0.8 g·L^{-1}; 8 ppm; 90 min	90% deg. ($NiFe_2O_4$@40% TiO_2)	[98]
$Co_{0.5}Zn_{0.25}M_{0.25}Fe_2O_4$/$TiO_2$ (M = Ni, Cu, Mn, Mg)	MO; MB	180 W solar simulator; 1 g·L^{-1}; 4·10^{-5} M; 80 min (MB) or 360 min (MO)	95% MO deg. ($Co_{0.5}Zn_{0.25}Ni_{0.25}Fe_2O_4$/$TiO_2$); 99% MB deg. ($Co_{0.5}Zn_{0.25}Ni_{0.25}Fe_2O_4$/$TiO_2$ and $Co_{0.5}Zn_{0.25}Mn_{0.25}Fe_2O_4$/$TiO_2$)	[99]

4-NPh—4-nitrophenol; conv.—conversion; deg.—degradation; ETD—etodolac; Hal.—halogen; MB—Methylene Blue; MO—Methyl Orange; Ph—phenol; TOC—total organic carbon.

It should be underlined that MFe_2O_4 NPs in TiO_2 composites (and in other ferromagnet-photocatalyst materials) can exhibit a dual function. First, as semiconductors with narrower bandgap than UV-active photocatalysts, they could take part in photocatalytic reactions, creating a heterojunction, which might cause both vis activity and efficient charge carriers' separation [100]. At the same time, their magnetic properties allow easy and cheap recycling of photocatalysts after reactions. However, in some cases, the direct connection between magnetic and photocatalytic materials is not worthwhile, especially when the separation is emphasized. For example, environmental conditions (e.g., acidic pH) and enhanced charge carrier migration (e.g., resulting in photocorrosion) could cause the leaching of iron ions from the composite, thus resulting in the destruction of the spinel ferrite structure. The possible reactions of Fe_3O_4 oxidation/reduction are presented in Equations (1)–(4) and Figure 5.

$$Fe^{3+}(s) + e^- \rightarrow Fe^{2+}(s) \quad (1)$$

$$Fe_2O_3 + 6H^+ + 2e^- \rightarrow 2Fe^{2+} + 3H_2O \quad (2)$$

$$Fe_3O_4 + 8H^+ + 3e^- \rightarrow 3Fe^{2+} + 4H_2O \quad (3)$$

$$Fe^{2+}(aq) + h^+ \rightarrow Fe^{3+}(aq) \quad (4)$$

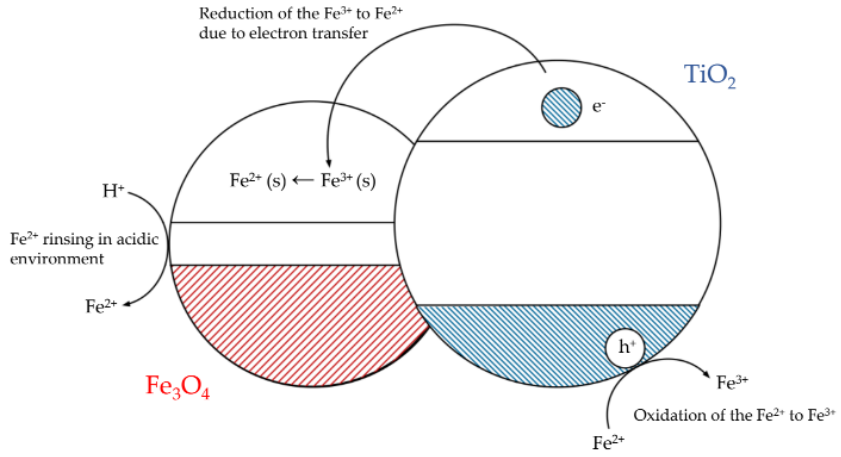

Figure 5. Possible reactions in Fe_3O_4/TiO_2 composite (drawn based on [101]).

Accordingly, the approach of separation between magnetic and photocatalytic parts through an inert interlayer, such as silica [102], polyaniline [103], and carbon [104], has been proposed. The core-interlayer-shell structure (e.g., shown in Figure 6), with a magnetic core, an inert interlayer, and a photocatalytic shell, prevents unfavorable charge transfer, maintaining the photocatalytic and magnetic properties of both composites.

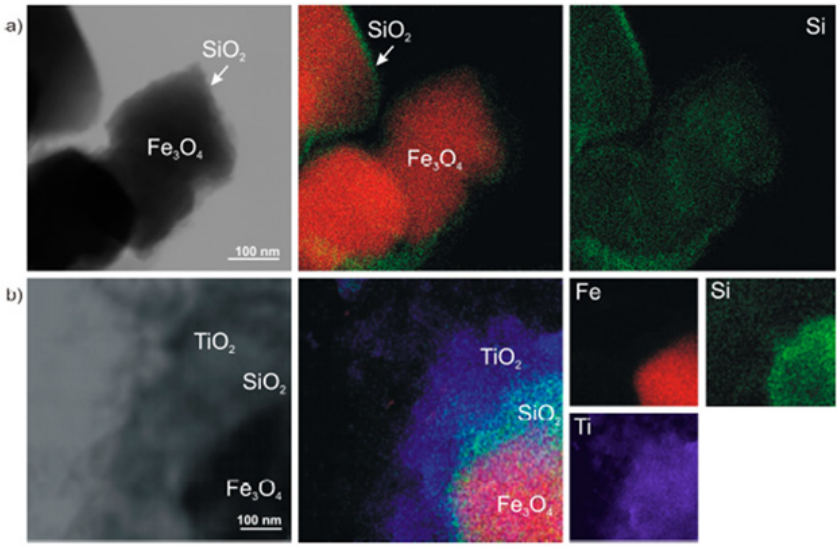

Figure 6. STEM images of Fe_3O_4@SiO_2 (**a**) and Fe_3O_4@SiO_2/TiO_2 (**b**) combined with Ti, Fe, and Si mapping. Reprinted with permission from [102]. Copyright (2017) Creative Commons Attribution.

4.2. Hexaferrites with TiO_2

Although pure hexaferrites have gained moderate attention as photocatalysts, their combination with other photoactive materials have frequently been reported. Among them, titania-based photocatalysts are the most common (see Table 4). For example, $BaFe_{12}O_{19}/TiO_2$ composites, initially reported by Fu et al. [105] and Lee et al. [106], can be prepared by a simple TiO_2 coating on the surface of the ferrite. In both studies, procion red MX 5B was used as a target pollutant decomposed under UV irradiation (no reusability analysis). It was found that though the activity increased with an increase in TiO_2 content, it was always lower than that of the P25 reference and/or sole TiO_2 NPs. In contrast, Xie et al. found higher activity for the $SrFe_{12}O_{19}/TiO_2$ composite (0.2/0.8 for Sr-ferrite and TiO_2, respectively) than that for single components under UV irradiation [107]. Moreover, reusability was also confirmed in three consecutive cycles, with an activity decrease of ca.

10%. Furthermore, in contrast to pristine TiO_2 NPs, the composites also exhibited activity under visible-light ($\lambda \geq 420$ nm) irradiation. In both cases (UV and visible-light irradiation), 100% degradation was observed after approx. 4–5 h of irradiation. It has been proposed that enhanced activity is caused by the possible formation of a n-n type heterojunction between both phases. Another $SrFe_{12}O_{19}$-based composite was also prepared by Bavarsiha et al. [108]. This time, three-phase composites, i.e., core/interlayer/shell structure, were prepared using $SrFe_{12}O_{19}$, SiO_2, and TiO_2 as a core, an interlayer, and an outerlayer, respectively. The efficiency of the composite was confirmed during degradation of MB, reaching ca. 80% degradation during 3 h of UV irradiation, with high reusability since only an 8% activity decrease was observed after three cycles. As a reference, $SrFe_{12}O_{19}/SiO_2$ composite was used, showing negligible photocatalytic activity. Finally, $PbFe_{12}O_{19}/TiO_2$ composite was also investigated by Lahijani et al. for degradation of Acid Blue 29, Acid Violet 7, and Acid Black 1 dyes [109]. The effective decolorization (based on the presented photographs) was observed for all tested dyes during 20−40 min of UV irradiation, but detailed process kinetics, as well as reusability, were not examined.

Table 4. Summary of TiO_2-hexaferrite photocatalysts.

Photocatalyst	Pollutants	Experimental Conditions	Findings	Ref.
$BaFe_{12}O_{19}/TiO_2$ (10–30% TiO_2)	Procion Red MX-5B	4 × 8 W UV bulbs (λ_{max} 365 nm); 0.2 g·L^{-1} (with respect to TiO_2); 10 ppm; 300 min	75% deg. ($BaFe_{12}O_{19}$); 96% deg. ($BaFe_{12}O_{19}$/30%TiO_2)	[105]
$BaFe_{12}O_{19}/TiO_2$			60% deg. ($BaFe_{12}O_{19}$/30%TiO_2 after 500 °C heat treatment); 70% deg. ($BaFe_{12}O_{19}$/30% TiO_2 without heat treatment);	[106]
$SrFe_{12}O_{19}/TiO_2$ (70–85% TiO_2 content)	MB	UV light (λ_{max} 254 nm) or vis light (λ > 420 nm); pH 7; 2 g·L^{-1}; 10 ppm; 300 min	95% deg. (UV) and 99% deg. (vis) for $SrFe_{12}O_{19}$/80% TiO_2	[107]
$SrFe_{12}O_{19}/SiO_2/TiO_2$	MB	20 W UV light; 50 ppm; 180 min	80% deg.	[108]
$PbFe_{12}O_{19}/TiO_2$	ABl; AV; ABk	10 W UV light; 20 g·L^{-1}; 10 ppm; 60 min	~100% dec. of all dyes	[109]

ABk—Acid Black 1; ABl—Acid Blue 29; AV—Acid Violet 7; dec.—decolorization; deg.—degradation; MB—Methylene Blue.

5. Other Magnetic-Photocatalytic Composites

Titania is still the main photocatalytic material used. However, the continuous development of materials science shows that the photocatalytic activity of titania depends on various parameters, including the crystal structure, the presence of surface impurities, the specific surface area, the morphology, etc. [4]. In order to be able to control the above parameters, it is necessary not only to apply innovative synthesis techniques (e.g., microwave route [110]) but also to use morphology-determining agents (e.g., hydrofluoric acid [111]). Despite the undoubted advantages resulting from the high photoactivity of titania, researchers are still looking for novel materials with similar or better parameters than TiO_2. However, regardless of the main component of the photocatalytic composite, e.g., ZnO [112], CuO [113], or others, the key aspect is the recovery of the material after the photodegradation process. Therefore, in the next part of this review, the current state of knowledge in the field of ferrite-based composite photocatalysts not containing titania is presented and discussed.

5.1. Spinel Ferrite Composites

The summary of selected materials containing spinel ferrites is presented in Table 5. Despite the semiconductor and ferrite types, all composites (presented in the Table 5) have

revealed high photocatalytic activity, in the range of 96% (ZnS-WO_3-$CoFe_2O_4$ [114] and $Ag_3PO_4/MnFe_2O_4$ [115]) to even 100% (rGO-based spinel ferrite composites [116,117]). It has also been proven by Abroshan et al. [115] that MB degradation for single-phase manganese spinel ferrites and trisilver phosphates is much lower than that for the composite (58%, 80%, and 96%, respectively), probably due to the formation of a heterojunction between the phases, allowing the effective charge separation.

Additionally, in a large number of research works, the recovery/recycling of the magnetic composites was investigated. The use of external magnetic field allows the genuine separation, and thus the reuse, of the photoactive material in at least three cycles of pollutant degradation. As a prominent example, in the work of Dudziak et al. [118], during eight cycles of carbamazepine photodegradation on the Fe_3O_4-based Pt-modified composite, 100% efficiency was preserved.

Table 5. Summary of selected spinel ferrite–photocatalyst composites.

Photocatalyst	Pollutants	Experimental Conditions	Findings	Ref.
$Ag_3PO_4/MnFe_2O_4$	MB; RhB	Sunlight (Iran, ~185 mW·cm^{-2}); 2 g·L^{-1}; 15 ppm; 80 min	58% MB deg. ($MnFe_2O_4$); 80% MB deg. (Ag_3PO_4); 96% MB deg. ($Ag_3PO_4/MnFe_2O_4$)	[115]
$Ni_{0.65}Zn_{0.35}Fe_2O_4$@rGO	MB	300 W Xe lamp (vis λ > 420 nm); 1 g·L^{-1}; 5 ppm; 48 min	100% dec.; 5 cycles—10% activity loss	[116]
$BiFeO_3$-$ZnFe_2O_4$	MB	100 W Xe lamp with cut-off filter (λ > 420 nm); pH 2; 1 g·L^{-1}; 15 ppm; 120 min	~97% deg. ($BiFeO_3$-25 wt% $ZnFe_2O_4$)	[119]
LaZF@rGO	RhB	UV lamp (λ_{max} = 254 nm; 0.6 mW·cm^{-2}); 1 mM PDS; pH 4.5; 0.25 g·L^{-1}; 30 ppm; 80 min	100% dec. (1:1 LaZF@rGO)	[117]
ZnS-WO_3-$CoFe_2O_4$	MB	Tungsten-halogen lamp (400–800 nm); 0.05 g; 50 ppm; 180 min	96% deg.; 4 cycles no activity loss	[114]
PANI/BiOBr/$ZnFe_2O_4$	RhB; NB	HPHgL with cut-off filter (λ > 420 nm); 1 g·L^{-1}; 20 ppm (RhB) and 5 ppm (NB); 30 min	99% RhB deg. & 87% NB red. (7% PANI/BiOBr/$ZnFe_2O_4$)	[120]

dec.—decolorization; HPHgL—high pressure mercury lamp; LaZF—lanthanum-substituted zinc spinel ferrite; MB—Methylene Blue; NB—nitrobenzene; PANI—polyaniline; PDS—peroxydisulfate; red.—reduction; rGO—reduced graphene oxide; RhB—Rhodamine B.

Carbon-based materials, i.e., containing graphene, reduced graphene oxide (rGO), carbon nanotubes (CNT) or graphitic carbon nitride, have recently been widely used for photocatalytic reactions. After coupling them with spinel ferrite NPs, an efficient composite with both photocatalytic activity and magnetic separability can be obtained. What is more important, the photogenerated electrons can migrate only from ferrite to carbon material. In this regard, the main shortcoming of a ferrite-based photocatalyst, i.e., photobleaching, is inhibited [63].

The schematic mechanism of heterojunction for non-carbon-based ferrites is shown in Figure 7, where $ZnFe_2O_4$ NPs and $BiFeO_3$ represent the group of p-type and n-type materials, respectively. It has been proposed that during visible-light irradiation, the excited electron from CB of $ZnFe_2O_4$ could migrate to CB of $BiFeO_3$. At the same time, the created holes are transferred between the valence bands, in the opposite direction, due striving for the equilibrium state. Accordingly, this separation of charge carriers might effectively improve the photoactivity of the composite [119].

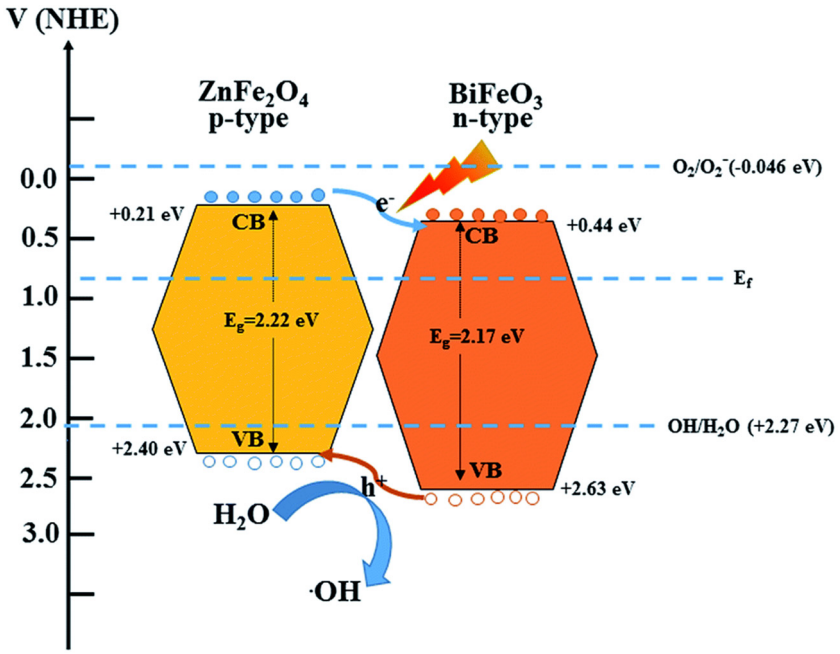

Figure 7. The schematic illustration of charge carriers' migration in $BiFeO_3$-$ZnFe_2O_4$ composite. Reprinted with permission from [119]. Copyright (2018) Creative Commons Attribution.

5.2. Hexaferrites Composites

Similar to spinel ferrites, hexaferrites have also been combined with different carbon-based materials, especially for possible visible-light response, as summarized in Table 6. For example, Mahdiani et al. investigated the photoactivity of $PbFe_{12}O_{19}$/graphene and $PbFe_{12}O_{19}$/CNT composites for degradation of methyl orange under UV irradiation and acidic conditions (pH 2–3) [121]. An increased activity of the composite in comparison to the simple $PbFe_{12}O_{19}$ structure, especially for the graphene-based photocatalyst, was explained by the inhibition of charge carriers' recombination, resulting from the separation of the π-π* orbitals of graphene due to the interactions with the 2p oxygen orbitals from the ferrite structure. Ultimately, 75% degradation efficiency was observed for $PbFe_{12}O_{19}$/graphene after 70 min of irradiation. A unique approach was proposed by Ismail et al., where $BaFe_{12}O_{19}$/g-C_3N_4 photocatalysts were used to reduce Hg(II) ions [122]. Although the photocatalysts contained only 1–4 mass% of Ba-ferrite, a significant activity increase was observed with respect to the sole $BaFe_{12}O_{19}$ and g-C_3N_4 materials. It was proposed that enhanced activity could be caused by charge carrier migration and cumulation on different components, i.e., electrons and holes on g-C_3N_4 and ferrite, respectively. The best activity was obtained for 3%-$BaFe_{12}O_{19}$ composite under vis irradiation ($\lambda > 420$ nm), reaching 100% reduction of Hg^{2+} ions within 30 min. Reusability of the composite was also tested, and a slight decrease in activity (from 100% to 90%) after five consecutive cycles was ascribed to be caused by the blocking of the surface active sites (no photocatalyst loss). Furthermore, Wang et al. also investigated $BaFe_{12}O_{19}$/g-C_3N_4 composites, using them as catalysts in the photo-Fenton process of rhodamine B degradation under visible-light irradiation [123]. Again, a synergistic effect was observed, with the highest activity achieved for 16.8 wt% of $BaFe_{12}O_{19}$. It was also proposed that charge separation between phases is responsible for the activity increase. However, in the contrast to the report by Ismail et al. [122], it was proposed that excited electrons react with H_2O_2 on the surface of $BaFe_{12}O_{19}$, whereas holes migrate to g-C_3N_4, as shown in Figure 8. Scavenger-based experiments have confirmed an active role of $^{\bullet}OH$, h^+ and $^{\bullet}O_2^-$ on the degradation efficiency. Reusability tests during four cycles showed a slight decrease in activity, from 98% to 91% degradation, during 100 min of irradiation. Quaternary composite $SrFe_{12}O_{19}/SiO_2/TiO_2$/GO was also proposed by Abd Aziz et al. towards direct sunlight-driven photocatalytic degradation of 2,4-dichlorophenol

(2,4-DCP) [124]. An increased activity of 4-phase composite in comparison to pristine TiO_2 and TiO_2/GO nanostructures was explained by the possible charge transfer between TiO_2 and GO and increased specific surface area of the composite. It was proposed that the ferrite contribution to the photocatalytic mechanism is insignificant because of its coverage with an insulating layer (SiO_2). Moreover, it was shown that photocatalysts could be efficiently reused, as complete degradation of 2.4-DCP was observed during three cycles within 2.5−5 h (depending on the light intensity) of sunlight irradiation.

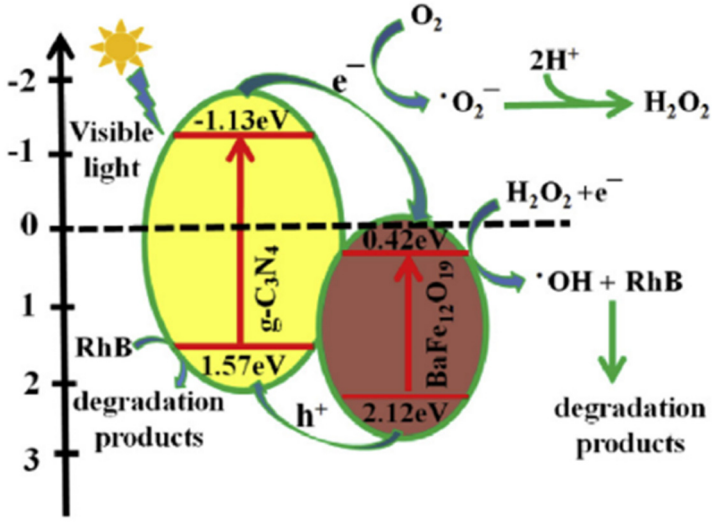

Figure 8. The schematic illustration of the proposed mechanism for the photocatalytic degradation of Rhodamine B on $BaFe_{12}O_{19}$ ferrite/g-C_3N_4 composite. Reprinted with permission from [123]. Copyright (2017) Elsevier.

Finally, hexagonal ferrites, combined with other photocatalysts, have also been intensively studied. For example, Xie et al. proposed a double-magnetic composite of $ZnFe_2O_4$/$SrFe_{12}O_{19}$ as a visible-light active photocatalyst towards the degradation of MB [125]. It was proposed that the composite exhibits both improved magnetic and photocatalytic performance, i.e., (i) $SrFe_{12}O_{19}$ enhances the magnetic properties of $ZnFe_2O_4$, which are quite weak for the pure spinel phase (M_S value of ca. 1.75 and 39 $Am^2 \cdot kg^{-1}$ for the pure $ZnFe_2O_4$ and the composite, respectively), and (ii) substitution of Fe^{3+} by Zn^{2+} ions at the 2a sites of the M-ferrite structure results in enhanced photocatalytic activity when compared to pristine $ZnFe_2O_4$. This substitution caused a presence of Fe^{2+} in the composite, and the resulting Fe^{2+}/Fe^{3+} interactions could be responsible for an increased e^- transport and a further increase in photocatalytic activity of the composite. However, reusability tests showed a constant decrease in activity between the first and fifth cycle (from 95% to 70% degradation), connected with possible photocatalyst loss between the cycles as well as surface blocking and partial destruction of the composite mesostructured. Another photocatalyst was designed by Sobhani-Nasab et al., who prepared a $BaFe_{12}O_{19}$/$Sm_2Ti_2O_7$ structure in its bare and Ag-decorated forms [126]. It was found that Ag has a positive impact on the activity, resulting in 100% degradation of MB during 150 min of vis irradiation (400–770 nm). It should be pointed out that the positive effect of noble metals has been well known and intensively investigated for more than forty years, as they usually work as an electron scavenger, inhibiting charge carriers' recombination [127–130]. Unfortunately, recycling causes a slight activity decrease (as in many ferrite-based photocatalysts), to 90% degradation after four cycles.

Another visible-light active structure was proposed by Xie et al., who prepared a $SrFe_{12}O_{19}$/BiOBr 2D-2D nanocomposite for the degradation of Rhodamine B ($\lambda > 420$ nm) [131]. An increase in the activity of BiOBr was noticed for samples with 3 wt% and 5 wt% Sr-ferrite, probably because of increased charge carrier separation, where electrons migrate

to BiOBr and holes to the $SrFe_{12}O_{19}$. The highest removal efficiency of 97% after 30 min of visible-light irradiation was achieved for the sample with 5 wt% of $SrFe_{12}O_{19}$. Similar to other ferrite photocatalysts, an activity loss (97% to ca. 90%) was observed during five cycles of degradation. Finally, scavenger-based experiments showed that $^{\bullet}OH$ radicals play a less significant role in the examined system than e^- and $^{\bullet}O_2^-$, which might suggest that the oxidative potential of h^+ at the ferrite surface might be too low to effectively oxidize water to $^{\bullet}OH$.

An interesting approach was suggested by Xu et al., in which $BaFe_{12}O_{19}$ ferrite was coupled with Ag_3PO_4 photocatalysts to create an in situ Fenton-like photosystem for degradation of bisphenol A under visible light ($\lambda \geq 420$ nm) [132]. It is known that Ag_3PO_4 is able to generate H_2O_2 due to 2-electron oxygen reduction (photocatalytic reaction); then, H_2O_2 is responsible for further degradation of organic pollutants [133]. An approach proposed by Xu et al. not only utilized $BaFe_{12}O_{19}$ as a magnetically separable part of the composite, but also enabled further conversion of photogenerated H_2O_2 to other reactive oxygen species (ROS), such as a $^{\bullet}OH$ and $^{\bullet}O_2^-$. The quantification of generated H_2O_2 for pristine Ag_3PO_4 and $Ag_3PO_4/BaFe_{12}O_{19}$ composite, as well as ESR-DMPO experiments for the observation of $^{\bullet}OH$ and $^{\bullet}O_2^-$ radicals, were used for the mechanism clarification. For 10% Ba-ferrite composite, the amount of both radicals was significantly increased, whereas the concentration of H_2O_2 was ca. three times lower than that of Ag_3PO_4. Unfortunately, the stability tests showed an efficiency decrease from 80% to ca. 60% after four cycles of 30 min of irradiation. Much worse stability was observed for pristine Ag_3PO_4, where a decrease in activity from 50% to ca. 5% was noticed (Photocorrosion of Ag_3PO_4 and $Ag_4P_2O_7$ is a well-known problem [134,135]). As another example of $BaFe_{12}O_{19}$ ferrite combined with an Ag-based photocatalyst, Xie et al. proposed a $BaFe_{12}O_{19}/AgBr$ composite for visible-light degradation of 2-mercaptobenzothiazole—MBT ($\lambda \geq 420$ nm) [136]. Again, the synergistic effect between both phases was observed, with the highest degradation efficiency (100% during 30 min) observed for the photocatalyst containing 10% $BaFe_{12}O_{19}$ ferrite. However, XPS analysis showed the presence of zero-valent silver (Ag^0), thus indicating the formation of a $BaFe_{12}O_{19}/AgBr/Ag$ ternary structure. The charge transfer and separation between these three components was recognized as a main reason behind the increased activity of the composite. Based on the combined Mott-Schottky and ESR-DMPO experiments, a Z-scheme heterojunction was proposed with (i) Ag^0 acting as an "intermediate" for electron transfer between $BaFe_{12}O_{19}$ and AgBr, (ii) oxygen reduction to $^{\bullet}O_2^-$ on AgBr, and (iii) H_2O oxidation to $^{\bullet}OH$ on $BaFe_{12}O_{19}$. The proposed mechanism is presented in Figure 9. The slight activity loss was observed during recycling, i.e., 90% degradation after four 30 min cycles (but still almost 100% for a 1 h process).

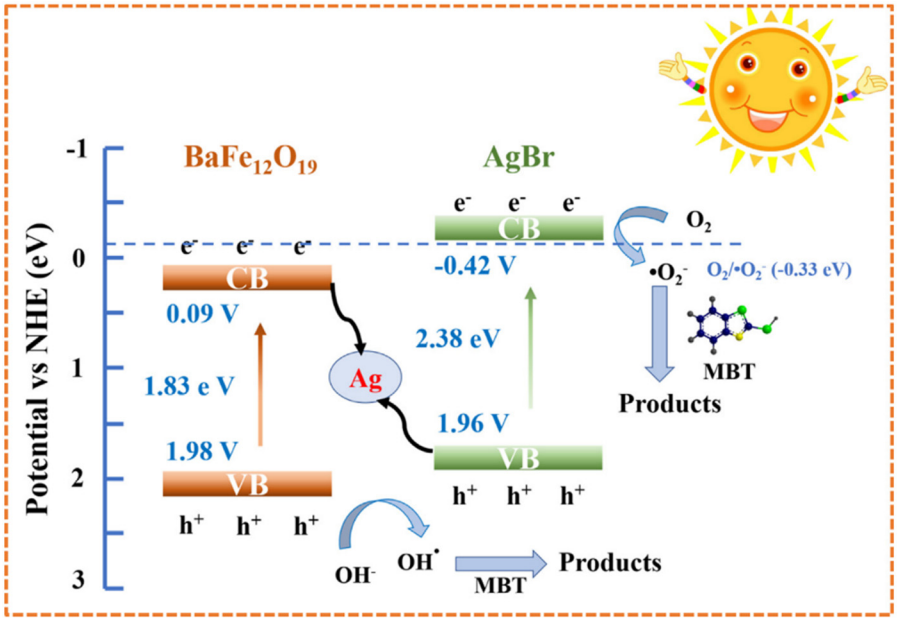

Figure 9. The schematic illustration of the proposed mechanism for degradation of 2-mercaptobenzothiazole over the ternary $BaFe_{12}O_{19}$/Ag/AgBr nanocomposite. Reprinted with permission from [136]. Copyright (2020) Elsevier.

In another study, Chen et al. prepared a $SrFe_{12}O_{19}/MoS_2$ heterostructure as the visible-light active photocatalysts for MB and methyl orange (MO) degradation under simulated sunlight [137]. The highest activity was observed for the composite with 1:2 mass ratio of Sr-ferrite:MoS_2, reaching ca. 100% and 70% degradation of MB (120 min) and MO (60 min). A possible charge separation between both phases was suggested, with electron and hole migration to $SrFe_{12}O_{19}$ and MoS_2, respectively, generating ROS ($^{\bullet}OH$ and $^{\bullet}O_2^-$). During six subsequent cycles of MB degradation, a decrease in activity to 82% was observed. However, XRD and XPS analyses did not reveal any significant change in the composite structure. Furthermore, $SrFe_{12}O_{19}$ was also coupled with Bi_2O_3 for MB degradation under visible-light irradiation ($\lambda > 420$ nm) [138]. It was found that an increase in Sr-ferrite content between 30% and 40% caused a photocatalytic activity increase, with a maximum efficiency obtained for 35% of $SrFe_{12}O_{19}$. The most important finding was the stable activity (100% degradation of MB during 4 h of irradiation) for three subsequent cycles. It was proposed that increased photocatalytic activity of the composite could be caused by three possible factors: (i) charge separation between both phases, with electrons accumulating on the Bi_2O_3 phase, (ii) increased mobility of the charge carriers inside the $SrFe_{12}O_{19}$ structure due to its remanent magnetic field, and (iii) increased light absorption efficiency by $SrFe_{12}O_{19}$ (when compared to pristine Bi_2O_3). Other composites utilizing different Bi-based photocatalysts were also investigated by Wang et al., combining $SrFe_{12}O_{19}$ ferrite with $Bi_4O_5Br_2$ and Bi_3O_4Cl [139,140]. During both studies, the composites were tested for degradation of Rhodamine B (10 ppm) under UV/vis irradiation (Xe lamp). The synergistic effect was observed between Sr-ferrite and $Bi_4O_5Br_2$ when the composite contained 5 wt% of $SrFe_{12}O_{19}$. However, there was no synergy between the components in the case of the $SrFe_{12}O_{19}/Bi_3O_4Cl$ photocatalyst. Ultimately, the 5 wt% Sr-ferrite/$Bi_4O_5Br_2$ was found to be the most active sample in both studies. It was proposed that an activity increase was caused by the charge carriers' separation, with electrons accumulating on the ferrite phase. Scavenger-based studies have shown the dominant role of $^{\bullet}O_2^-$ radicals and an insignificant contribution of $^{\bullet}OH$. The latter might relate to the unsuitable position of the valence band edge for both components. The reusability tests for five consecutive cycles indicated a constant activity decrease (from 100% to 85% of degradation). Although it has been proposed that an activity decrease is caused by the composite loss during the

recovery, the constant change in the reaction rates between the cycles might also suggest that some damage could occur directly during the process.

Moreover, a novel structure, based on $SrFe_{12}O_{19}$ ferrite, carbon quantum dots (CQDs) and CeO_2, was proposed by Wang et al. [141]. The ternary composite allows an increase in both the adsorption efficiency of pollutants (here MB) and photocatalytic efficiency under simulated sunlight (AM1.5), when compared to pristine CeO_2, CeO_2/CQDs, and $SrFe_{12}O_{19}/CeO_2$ materials. It was proposed that the formation of II-type heterojunction between Sr-ferrite and Ce_2O is responsible for enhanced photocatalytic activity. Ternary composite could decompose 90% of MB during 4 hours of irradiation, but a decrease in activity to 65% was observed after four subsequent cycles.

Finally, hexagonal ferrites have also been combined with conjugated polymers, such as polyaniline (PANI) and polythiophene (PTh). For example, Mesdaghi et al. prepared two composite systems using Zn,Co,Sn-co-doped $BaFe_{12}O_{19}$ ferrite with either multiwall carbon nanotubes (MWCNTs) or polyaniline [142]. The composites, tested towards degradation of MB under irradiation with an Hg lamp ($\lambda > 400$ nm), showed increased activity in comparison to the pure ferrite; however, MWCT-based composite slightly outperformed the PANI-based one. In both cases, a decrease in degradation efficiency was observed after the three degradation cycles. A similar study was also performed by Khandani et al., who combined Ce,Nd-co-doped $SrFe_{12}O_{19}$ ferrite with polythiophene [142]. Again, the combination of ferrite with polymer increased the degradation efficiency (MB) by ca. two times. However, it should be noted that, during both studies, the composition of both phases was not optimized, and the mechanism of the photocatalytic reaction was not examined in detail.

Table 6. Summary of hexaferrite-photocatalyst composites.

Photocatalyst	Pollutants	Experimental Conditions	Findings	Ref.
$CdFe_{12}O_{19}/CdTiO_3$	MO; MB; MV	400 W UV light; 1 $g \cdot L^{-1}$; 5 ppm; 70 min	71% deg. MO; 61% deg. MB; 55 deg. MV	[83]
$PbFe_{12}O_{19}$/GN and $PbFe_{12}O_{19}$/CNT	MO	UV light; pH 2–3	75% deg. ($PbFe_{12}O_{19}$/GN); 50% deg. ($PbFe_{12}O_{19}$/CNT)	[121]
$BaFe_{12}O_{19}/g\text{-}C_3N_4$	Hg^{2+}	Xe lamp ($\lambda > 420$ nm; 425 $W \cdot m^{-2}$); pH 4; 0.4–2 $g \cdot L^{-1}$; 100 ppm; 30 min	100% red. of Hg^{2+} ions	[122]
$BaFe_{12}O_{19}/g\text{-}C_3N_4$ (10.1–35.5% wt. of Ba-ferrite)	RhB	Vis light; T = 30°C; 1 $g \cdot L^{-1}$; 10 ppm; 40 min; 0.5 ml of 30% H_2O_2	17% deg. (10.1% $BaFe_{12}O_{19}/g\text{-}C_3N_4$); 86% deg. (16.8% $BaFe_{12}O_{19}/g\text{-}C_3N_4$)	[123]
$SrFe_{12}O_{19}/SiO_2/TiO_2$/GO	2,4-DCP	Kuala Lumpur sunlight; 482–776 $W \cdot m^{-2}$; 2 $g \cdot L^{-1}$; 50 ppm; 170–300 min	100% deg.; time depending on sunlight intensity (180 min—776 $W \cdot m^{-2}$; 300 min—482 $W \cdot m^{-2}$)	[124]
$SrFe_{12}O_{19}/ZnFe_2O_4$	MB	500 W Xe lamp; pH 7; 2 $g \cdot L^{-1}$; 10 ppm; 300 min	97% deg.	[125]
$BaFe_{12}O_{19}/Sm_2Ti_2O_7$/Ag (0–20% Ag salt)	MB	400 W lamp (400–770 nm); 10 ppm; 150 min	45% deg. ($BaFe_{12}O_{19}/Sm_2Ti_2O_7$); 100% deg. ($BaFe_{12}O_{19}/Sm_2Ti_2O_7$/20% Ag)	[126]
$SrFe_{12}O_{19}$/BiOBr (3–15% wt. of Sr-ferrite)	RhB	300 W Xe lamp, filter ($\lambda > 420$ nm); 0.5 $g \cdot L^{-1}$; 10 ppm; 30 min	55% deg. (15% $SrFe_{12}O_{19}$/BiOBr); 97% deg. (5% $SrFe_{12}O_{19}$/BiOBr)	[131]

Table 6. *Cont.*

Photocatalyst	Pollutants	Experimental Conditions	Findings	Ref.
$BaFe_{12}O_{19}/Ag_3PO_4$ (1–15% wt. of Ba-ferrite)	BPhA	300 W Xe lamp ($\lambda \geq 420$ nm); 1 $g \cdot L^{-1}$; 20 ppm; 30 min	53% deg. (1% $BaFe_{12}O_{19}/Ag_3PO_4$); 80% deg. (10% $BaFe_{12}O_{19}/Ag_3PO_4$)	[132]
$BaFe_{12}O_{19}$/AgBr/Ag (1–20% wt. of Ba-ferrite)	MBT	300 W Xe lamp filter ($\lambda > 420$ nm); 1 $g \cdot L^{-1}$; 20 ppm; 30 min	~72% deg. (1% $BaFe_{12}O_{19}$/AgBr/Ag); 98% deg. (10% $BaFe_{12}O_{19}$/AgBr/Ag)	[136]
$SrFe_{12}O_{19}/MoS_2$ (66% and 75% wt. of MoS_2)	MB; MO	Simulated sunlight; 0.375 $g \cdot L^{-1}$; 20 ppm; 120 min (MB) or 60 min (MO)	86% MB deg. & 61% MO deg. ($SrFe_{12}O_{19}$/66% MoS_2)	[137]
$SrFe_{12}O_{19}/Bi_2O_3$ (20–40% wt. of Sr-ferrite)	MB	500 W Hg lamp ($\lambda > 420$ nm; 1111 $W \cdot m^{-2}$); pH 7; 2 $g \cdot L^{-1}$; 10 ppm; 240 min	~28% deg. (20% $SrFe_{12}O_{19}/Bi_2O_3$); 95% deg. (35% $SrFe_{12}O_{19}/Bi_2O_3$)	[138]
$SrFe_{12}O_{19}/CeO_2$/CQDs	MB	500 W Xe lamp with AM1.5 filter; 0.2–1.8 $g \cdot L^{-1}$; 1–10 ppm; 240 min	90% deg.	[141]
$SrFe_{12}O_{19}/Bi_3O_4Cl$ (5–25% wt. of Sr-ferrite)	RhB	300 W Xe lamp; 1 $g \cdot L^{-1}$, 10 ppm, 80 min	~15% deg. (bare $SrFe_{12}O_{19}$); 100% deg. (5% $SrFe_{12}O_{19}$);	[139]
$SrFe_{12}O_{19}/Bi_4O_5Br_2$ (5–15% wt. of Sr-ferrite)	RhB	300 W Xe lamp; 1 $g \cdot L^{-1}$, 10 ppm, 60 min	~90% deg. (15% $SrFe_{12}O_{19}$) 100% deg. (5% $SrFe_{12}O_{19}$)	[140]
$BaZn_{0.2}Co_{0.2}Sn_{0.4}Fe_{11.2}O_{19}$ with MWCNT or PANI	MB	800 W Hg lamp ($\lambda > 400$ nm); 20 ppm, 60 min	87% deg. with MWCNT; 80% deg. with PANI	[142]
$SrCe_{0.2}Nd_{0.2}Fe_{11.6}O_{19}$/PTh (33% or 66% wt. of PTh)	MB	800 W Hg lamp ($\lambda > 400$ nm); 2 g·L-1, 10 ppm, 30 min	95% deg. (66% wt. of PTh); 75% deg. (33% wt. of PTh)	[143]

2,4-DCP—2,4-dichlorophenol; BPhA—Bisphenol A; CNT—carbon nanotubes; CQDs—Carbon Quantum Dots; deg.—degradation; GN—graphene; GO—graphene oxide; MB—Methylene Blue; MBT—2-mercaptobenzothiazole; MO—Methyl Orange; MV—Methyl Violet; MWCNT—multi-walled carbon nanotubes; PANI—polyaniline; PTh—polythiophene; red.—reduction; RhB—Rhodamine B.

6. Conclusions and Future Perspectives

The literature review reflects the recent need to search for innovative combinations of semiconductors with ferrite NPs for heterogeneous photocatalysis. Various studies have been carried out at multiple research centers worldwide, being largely focused on the choice of appropriate ferromagnets to produce advanced magnetic photocatalytic systems. Based on the presented literature, it was found that spinel and hexagonal ferrite magnetic NPs, despite their magnetic properties enabling easy separation, have received moderate attention as the main photocatalytic material, probably because of lower activity than well-known photocatalysts (e.g., TiO_2) and stability concerns. However, they could be an interesting component of photocatalytic materials, with a possible synergistic effect, resulting in increased activity under UV light and the appearance of vis response. However, their stability (even though, in many cases, it is much better than single-component photocatalysts) should be improved for possible commercialization, as most lose activity during recycling.

Moreover, though ferrites have proven to be a suitable choice for the separation of the multi-phase photocatalysts, there are still some unknown aspects of their operation in the photocatalytic systems. Above all, the ability of the ferrite materials to generate reactive oxygen species by themselves; as well, further identification of the main ROS and the positions of CB and VB edges of such ferrite materials are usually missing. This leads

to confusing results reported in different studies. For example, opposite charge transfers between the same components was claimed (e.g., $BaFe_{12}O_{19}/g\text{-}C_3N_4$ [122,123]) or the oxidative role of $^{\bullet}OH$ radicals in the presence of Ba-ferrite [78,81] was suggested, whereas other studies excluded such mechanisms [131,137]. Since water purification from organic pollutants remains the most investigated application of the magnetic photocatalysts, these details, as well as the possible factors that affect them, are considered as crucial for further studies to better understand the interactions between hexaferrites, other photocatalysts, and pollutants. Moreover, the surface structure of the magnetic materials is usually not considered, though many reports on other photocatalysts have proven how important it is for efficient photocatalytic performance [111,144]. In this regard, surface-based studies of such materials are highly recommended as another direction for further research.

It is also thought that the mechanism of ferrite-based photocatalysts needs further investigation, as only a few studies discussed the possible mechanism in detail (showing direct proof instead of speculation). Moreover, though the use of dyes is very convenient for fast and easy activity testing (and important for environmental purification), it is not recommended for mechanism discussion due to the additional mechanisms of photocatalyst sensitization (barely discussed in the presented papers).

Even though there are many unsolved issues and unknown aspects, it is thought that the study of the creation of a new generation of ferromagnetic-photocatalytic systems will grow as a result of evolving strategies for environmental protection, since easy and inexpensive separation of photocatalysts for reuse is highly important.

Author Contributions: Writing—original draft preparation, S.D., A.K., Z.B. and E.K.; Writing—review and editing, S.D., A.K., Z.B. and E.K. All authors have read and agreed to the published version of the manuscript.

Funding: This research received no external funding.

Institutional Review Board Statement: Not applicable.

Informed Consent Statement: Not applicable.

Data Availability Statement: Data are available in a publicly accessible repository.

Conflicts of Interest: The authors declare no conflict of interest.

References

1. Roberts, B.A.; Strauss, C.R. Toward Rapid, "Green", Predictable Microwave-Assisted Synthesis. *ChemInform* **2005**, *36*, 653–661. [CrossRef]
2. Janczarek, M.; Kowalska, E. On the Origin of Enhanced Photocatalytic Activity of Copper-Modified Titania in the Oxidative Reaction Systems. *Catalysts* **2017**, *7*, 317. [CrossRef]
3. Siwińska-Stefańska, K.; Kubiak, A.; Piasecki, A.; Dobrowolska, A.; Czaczyk, K.; Motylenko, M.; Rafaja, D.; Ehrlich, H.; Jesionowski, T. Hydrothermal synthesis of multifunctional TiO_2-ZnO oxide systems with desired antibacterial and photocatalytic properties. *Appl. Surf. Sci.* **2019**, *463*, 791–801. [CrossRef]
4. Kubiak, A.; Siwińska-Ciesielczyk, K.; Jesionowski, T. Titania-Based Hybrid Materials with ZnO, ZrO_2 and MoS_2: A Review. *Materials* **2018**, *11*, 2295. [CrossRef]
5. Fujishima, A.; Honda, K. Electrochemical Photolysis of Water at Semiconductor Electrode. *Nature* **1972**, *238*, 37–38. [CrossRef] [PubMed]
6. Herrmann, J.M.; Disdier, J.; Pichat, P. Photoassisted platinum deposition on TiO_2 powder using various platinum complexes. *J. Phys. Chem.* **1986**, *90*, 6028–6034. [CrossRef]
7. Di Paola, A.; Marcì, G.; Palmisano, L.; Schiavello, M.; Uosaki, K.; Ikeda, S.; Ohtani, B. Preparation of polycrystalline TiO_2 photocatalysts impregnated with various transition metal ions: Characterization and photocatalytic activity for the degradation of 4-nitrophenol. *J. Phys. Chem. B* **2002**, *106*, 637–645. [CrossRef]
8. Zhang, L.; Baumanis, C.; Robben, L.; Kandiel, T.; Bahnemann, D. Bi_2WO_6 Inverse Opals: Facile Fabrication and Efficient Visible-Light-Driven Photocatalytic and Photoelectrochemical Water-Splitting Activity. *Small* **2011**, *7*, 2714–2720. [CrossRef]
9. Sclafani, A.; Palmisano, L.; Davì, E. Photocatalytic degradaton of phenol in aqueous polycrystalline TiO_2 dispersions: The influence of Fe3+, Fe^{2+} and Ag^{+} on the reaction rate. *J. Photochem. Photobiol. A Chem.* **1991**, *56*, 113–123. [CrossRef]
10. Hitoki, G.; Takata, T.; Kondo, J.N.; Hara, M.; Kobayashi, H.; Domen, K. An oxynitride, TaON, as an efficient water oxidation photocatalyst under visible light irradiation ($\lambda \leq 500$ nm). *Chem. Commun.* **2002**, *2*, 1698–1699. [CrossRef]

11. Tomita, O.; Nitta, S.; Matsuta, Y.; Hosokawa, S.; Higashi, M.; Abe, R. Improved photocatalytic water oxidation with Fe^{3+}/Fe^{2+} redox on rectangular-shaped WO_3 particles with specifically exposed crystal faces via hydrothermal synthesis. *Chem. Lett.* **2017**, *46*, 221–224. [CrossRef]
12. Buchalska, M.; Kuncewicz, J.; Świętek, E.; Łabuz, P.; Baran, T.; Stochel, G.; Macyk, W. Photoinduced hole injection in semiconductor-coordination compound systems. *Coord. Chem. Rev.* **2013**, *257*, 767–775. [CrossRef]
13. Kowalska, E.; Abe, R.; Ohtani, B. Visible light-induced photocatalytic reaction of gold-modified titanium(IV) oxide particles: Action spectrum analysis. *Chem. Commun.* **2009**, *2*, 241–243. [CrossRef]
14. Mitoraj, D.; Kisch, H. The nature of nitrogen-modified titanium dioxide photocatalysts active in visible light. *Angew. Chem. Int. Ed.* **2008**, *47*, 9975–9978. [CrossRef]
15. Ghosh, S.; Kouamé, N.A.; Ramos, L.; Remita, S.; Dazzi, A.; Deniset-Besseau, A.; Beaunier, P.; Goubard, F.; Aubert, P.H.; Remita, H. Conducting polymer nanostructures for photocatalysis under visible light. *Nat. Mater.* **2015**, *14*, 505–511. [CrossRef]
16. Dijkstra, M.F.J.; Michorius, A.; Buwalda, H.; Panneman, H.J.; Winkelman, J.G.M.; Beenackers, A.A.C.M. Comparison of the efficiency of immobilized and suspended systems in photocatalytic degradation. *Catal. Today* **2001**, *66*, 487–494. [CrossRef]
17. O'Neal Tugaoen, H.; Garcia-Segura, S.; Hristovski, K.; Westerhoff, P. Compact light-emitting diode optical fiber immobilized TiO_2 reactor for photocatalytic water treatment. *Sci. Total Environ.* **2018**, *613–614*, 1331–1338. [CrossRef]
18. Kubiak, A.; Żółtowska, S.; Bartkowiak, A.; Gabała, E.; Sacharczuk, N.; Zalas, M.; Siwińska-Ciesielczyk, K.; Jesionowski, T. The TiO_2-ZnO Systems with Multifunctional Applications in Photoactive Processes—Efficient Photocatalyst under UV-LED Light and Electrode Materials in DSSCs. *Materials* **2021**, *14*, 6063. [CrossRef]
19. Song, Y.; Ling, L.; Westerhoff, P.; Shang, C. Evanescent waves modulate energy efficiency of photocatalysis within TiO_2 coated optical fibers illuminated using LEDs. *Nat. Commun.* **2021**, *12*, 4101. [CrossRef] [PubMed]
20. Marques, A.C.; Vale, M.; Vicente, D.; Schreck, M.; Tervoort, E.; Niederberger, M. Porous Silica Microspheres with Immobilized Titania Nanoparticles for In-Flow Solar-Driven Purification of Wastewater. *Glob. Chall.* **2021**, *5*, 2000116. [CrossRef]
21. Verma, A.; Dixit, D.; Toor, A.; Srivastava, J. Heterogeneous Photocatalytic Degradation of 2-chloro-4-Nitrophenol Using Slurry and Fixed Bed Reactor. *Environ. Prog. Sustain. Energy* **2015**, *34*, 380–386. [CrossRef]
22. Villacres, R.; Ikeda, S.; Torimoto, T.; Ohtani, B. Development of a novel photocatalytic reaction system for oxidative decomposition of volatile organic compounds in water with enhanced aeration. *J. Photochem. Photobiol. A Chem.* **2003**, *160*, 121–126. [CrossRef]
23. Zielińska-Jurek, A.; Klein, M.; Hupka, J. Enhanced visible light photocatalytic activity of Pt/I-TiO_2 in a slurry system and supported on glass packing. *Sep. Purif. Technol.* **2017**, *189*, 246–252. [CrossRef]
24. Molinari, R.; Mungari, M.; Drioli, E.; Di Paola, A.; Loddo, V.; Palmisano, L.; Schiavello, M. Study on a photocatalytic membrane reactor for water purification. *Catal. Today* **2000**, *55*, 71–78. [CrossRef]
25. Mozia, S.; Tomaszewska, M.; Morawski, A.W. A new photocatalytic membrane reactor (PMR) for removal of azo-dye Acid Red 18 from water. *Appl. Catal. B Environ.* **2005**, *59*, 131–137. [CrossRef]
26. Argurio, P.; Fontananova, E.; Molinari, R.; Drioli, E. Photocatalytic membranes in photocatalytic membrane reactors. *Processes* **2018**, *6*, 162. [CrossRef]
27. Byrne, J.A.; Eggins, B.R.; Brown, N.M.D.; McKinney, B.; Rouse, M. Immobilisation of TiO_2 powder for the treatment of polluted water. *Appl. Catal. B Environ.* **1998**, *17*, 25–36. [CrossRef]
28. Chen, D.; Ray, A.K. Photocatalytic kinetics of phenol and its derivatives over UV irradiated TiO_2. *Appl. Catal. B Environ.* **1999**, *23*, 143–157. [CrossRef]
29. Arabatzis, I.M.; Stergiopoulos, T.; Bernard, M.C.; Labou, D.; Neophytides, S.G.; Falaras, P. Silver-modified titanium dioxide thin films for efficient photodegradation of methyl orange. *Appl. Catal. B Environ.* **2003**, *42*, 187–201. [CrossRef]
30. Markowska-Szczupak, A.; Rokicka, P.; Wang, K.; Endo, M.; Morawski, A.W.; Kowalska, E. Photocatalytic water disinfection under solar irradiation by D-glucose-modified titania. *Catalysts* **2018**, *8*, 316. [CrossRef]
31. Kowalska, E.; Rau, S. Photoreactors for Wastewater Treatment: A Review. *Recent Pat. Eng.* **2010**, *4*, 242–266. [CrossRef]
32. Kagaya, S.; Shimizu, K.; Arai, R.; Hasegawa, K. Separation of titanium dioxide photocatalyst in its aqueous suspensions by coagulation with basic aluminium chloride. *Water Res.* **1999**, *33*, 1753–1755. [CrossRef]
33. Baran, W.; Makowski, A.; Wardas, W. The separation of catalyst after photocatalytic reactions conducted in the presence of TiO2/FeCl3/UV. *Chemosphere* **2005**, *59*, 853–859. [CrossRef]
34. Wang, H.; Qi, J.; Keller, A.A.; Zhu, M.; Li, F. Effects of pH, ionic strength and humic acid on the removal of TiO_2 nanoparticles from aqueous phase by coagulation. *Colloids Surf. A Physicochem. Eng. Asp.* **2014**, *450*, 161–165. [CrossRef]
35. You, Z.; Zhuang, C.; Sun, Y.; Zhang, S.; Zheng, H. Efficient Removal of TiO_2 nanoparticles by enhanced flocculation-coagulation. *Ind. Eng. Chem. Res.* **2019**, *58*, 14528–14537. [CrossRef]
36. Xue, X.D.; Fu, J.F.; Zhu, W.F.; Guo, X.C. Separation of ultrafine TiO_2 from aqueous suspension and its reuse using cross-flow ultrafiltration (CFU). *Desalination* **2008**, *225*, 29–40. [CrossRef]
37. Chang, Y.; He, P.; Wei, Z.; Chen, Y.; Wang, H.; Wu, C.; Zhou, Z.; Huang, H.; Kowalska, E.; Dong, S. Three-dimensional monodispersed TiO_2 microsphere network formed by a sub-zero sol-gel method. *Mater. Lett.* **2020**, *268*, 127592. [CrossRef]
38. Gołąbiewska, A.; Checa-Suárez, M.; Paszkiewicz-Gawron, M.; Lisowski, W.; Raczuk, E.; Klimczuk, T.; Polkowska, Ż.; Grabowska, E.; Zaleska-Medynska, A.; Łuczak, J. Highly Active TiO_2 Microspheres Formation in the Presence of Ethylammonium Nitrate Ionic Liquid. *Catalysts* **2018**, *8*, 279. [CrossRef]

39. Shamaila, S.; Sajjad, A.K.L.; Chen, F.; Zhang, J. Study on highly visible light active Bi_2O_3 loaded ordered mesoporous titania. *Appl. Catal. B Environ.* **2010**, *94*, 272–280. [CrossRef]
40. Kubiak, A.; Kubacka, M.; Gabała, E.; Dobrowolska, A.; Synoradzki, K.; Siwińska-Ciesielczyk, K.; Czaczyk, K.; Jesionowski, T. Hydrothermally assisted fabrication of TiO_2-Fe_3O_4 composite materials and their antibacterial activity. *Materials* **2020**, *13*, 4715. [CrossRef]
41. Li, Z.-D.; Wang, H.-L.; Wei, X.-N.; Liu, X.-Y.; Yang, Y.-F.; Jiang, W.-F. Preparation and photocatalytic performance of magnetic Fe_3O_4@TiO_2 core-shell microspheres supported by silica aerogels from industrial fly ash. *J. Alloys Compd.* **2016**, *659*, 240–247. [CrossRef]
42. Li, W.; Deng, Y.; Wu, Z.; Qian, X.; Yang, J.; Wang, Y.; Gu, D.; Zhang, F.; Tu, B.; Zhao, D. Hydrothermal Etching Assisted Crystallization: A Facile Route to Functional Yolk-Shell Titanate Microspheres with Ultrathin Nanosheets-Assembled Double Shells. *J. Am. Chem. Soc.* **2011**, *133*, 15830–15833. [CrossRef]
43. Casbeer, E.; Sharma, V.K.; Li, X.Z. Synthesis and photocatalytic activity of ferrites under visible light: A review. *Sep. Purif. Technol.* **2012**, *87*, 1–14. [CrossRef]
44. Lisovski, O.; Piskunov, S.; Bocharov, D.; Kenmoe, S. 2D Slab Models of Nanotubes Based on Tetragonal TiO_2 Structures: Validation over a Diameter Range. *Nanomaterials* **2021**, *11*, 1925. [CrossRef]
45. Hu, L.; Xu, C.; Peng, L.; Gu, F.L.; Yang, W. Photocatalytic activity and the radiative lifetimes of excitons via an ab initio approach. *J. Mater. Chem. A* **2018**, *6*, 15027–15032. [CrossRef]
46. Lin, Y.-M.; Jiang, Z.-Y.; Zhu, C.-Y.; Hu, X.-Y.; Zhang, X.-D.; Fan, J. Visible-light photocatalytic activity of Ni-doped TiO_2 from ab initio calculations. *Mater. Chem. Phys.* **2012**, *133*, 746–750. [CrossRef]
47. Bocharov, D.; Piskunov, S.; Zhukovskii, Y.F.; Evarestov, R.A. Ab Initio Calculations on the Electronic Structure and Photocatalytic Properties of Two-Dimensional WS_2 (0001) Nanolayers of Varying Thickness. *Phys. Status Solidi Rapid Res. Lett.* **2018**, *13*, 1800253. [CrossRef]
48. Eidsvåg, H.; Bentouba, S.; Vajeeston, P.; Yohi, S.; Velauthapillai, D. TiO_2 as a photocatalyst for water splitting—An experimental and theoretical review. *Molecules* **2021**, *26*, 1687. [CrossRef]
49. Kefeni, K.K.; Msagati, T.A.M.; Mamba, B.B. Ferrite nanoparticles: Synthesis, characterisation and applications in electronic device. *Mater. Sci. Eng. B* **2017**, *215*, 37–55. [CrossRef]
50. Šutka, A.; Gross, K.A. Spinel ferrite oxide semiconductor gas sensors. *Sens. Actuators B Chem.* **2016**, *222*, 95–105. [CrossRef]
51. Sharifi, I.; Shokrollahi, H.; Amiri, S. Ferrite-based magnetic nanofluids used in hyperthermia applications. *J. Magn. Magn. Mater.* **2012**, *324*, 903–915. [CrossRef]
52. Amiri, M.; Salavati-Niasari, M.; Akbari, A. Magnetic nanocarriers: Evolution of spinel ferrites for medical applications. *Adv. Colloid Interface Sci.* **2019**, *265*, 29–44. [CrossRef]
53. Reddy, D.H.K.; Yun, Y.-S. Spinel ferrite magnetic adsorbents: Alternative future materials for water purification? *Coord. Chem. Rev.* **2016**, *315*, 90–111. [CrossRef]
54. Tatarchuk, T.; Paliychuk, N.; Bitra, R.B.; Shyichuk, A.; Naushad, M.; Mironyuk, I.; Ziółkowska, D. Adsorptive removal of toxic Methylene Blue and Acid Orange 7 dyes from aqueous medium using cobalt-zinc ferrite nanoadsorbents. *Desalin. Water Treat.* **2019**, *150*, 374–385. [CrossRef]
55. Tatarchuk, T.; Myslin, M.; Mironyuk, I.; Bououdina, M.; Pędziwiatr, A.T.; Gargula, R.; Bogacz, B.F.; Kurzydło, P. Synthesis, morphology, crystallite size and adsorption properties of nanostructured Mg–Zn ferrites with enhanced porous structure. *J. Alloys Compd.* **2020**, *819*, 152945. [CrossRef]
56. Wang, Y.; Zhao, H.; Li, M.; Fan, J.; Zhao, G. Magnetic ordered mesoporous copper ferrite as a heterogeneous Fenton catalyst for the degradation of imidacloprid. *Appl. Catal. B Environ.* **2014**, *147*, 534–545. [CrossRef]
57. Guan, Y.-H.; Ma, J.; Ren, Y.-M.; Liu, Y.-L.; Xiao, J.-Y.; Lin, L.; Zhang, C. Efficient degradation of atrazine by magnetic porous copper ferrite catalyzed peroxymonosulfate oxidation via the formation of hydroxyl and sulfate radicals. *Water Res.* **2013**, *47*, 5431–5438. [CrossRef]
58. Kharisov, B.I.; Dias, H.V.R.; Kharissova, O.V. Mini-review: Ferrite nanoparticles in the catalysis. *Arab. J. Chem.* **2019**, *12*, 1234–1246. [CrossRef]
59. Goyal, A.; Bansal, S.; Singhal, S. Facile reduction of nitrophenols: Comparative catalytic efficiency of MFe_2O_4 (M = Ni, Cu, Zn) nano ferrites. *Int. J. Hydrog. Energy* **2014**, *39*, 4895–4908. [CrossRef]
60. Pham, T.N.; Huy, T.Q.; Le, A.T. Spinel ferrite (AFe_2O_4)-based heterostructured designs for lithium-ion battery, environmental monitoring, and biomedical applications. *RSC Adv.* **2020**, *10*, 31622–31661. [CrossRef]
61. Serga, V.; Burve, R.; Maiorov, M.; Krumina, A.; Skaudžius, R.; Zarkov, A.; Kareiva, A.; Popov, A.I. Impact of Gadolinium on the Structure and Magnetic Properties of Nanocrystalline Powders of Iron Oxides Produced by the Extraction-Pyrolytic Method. *Materials* **2020**, *13*, 4147. [CrossRef]
62. Tatarchuk, T.R.; Bououdina, M.; Paliychuk, N.D.; Yaremiy, I.P.; Moklyak, V.V. Structural characterization and antistructure modeling of cobalt-substituted zinc ferrites. *J. Alloys Compd.* **2017**, *694*, 777–791. [CrossRef]
63. Janczarek, M.; Endo-Kimura, M.; Wei, Z.; Bielan, Z.; Mogan, T.R.; Khedr, T.M.; Wang, K.; Markowska-Szczupak, A.; Kowalska, E. Novel Structures and Applications of Graphene-Based Semiconductor Photocatalysts: Faceted Particles, Photonic Crystals, Antimicrobial and Magnetic Properties. *Appl. Sci.* **2021**, *11*, 1982. [CrossRef]

64. Gu, F.; Leshuk, T.; Linley, S. Superparamagnetic Photocatalytic Microparticles. U.S. Patent No. US 2014/0131288 A1, 17 May 2012. pp. 1–25.
65. Zhang, S.; Zhao, X.; Niu, H.; Shi, Y.; Cai, Y.; Jiang, G. Superparamagnetic Fe_3O_4 nanoparticles as catalysts for the catalytic oxidation of phenolic and aniline compounds. *J. Hazard. Mater.* **2009**, *167*, 560–566. [CrossRef]
66. Dudziak, S.; Ryzynska, Z.; Bielan, Z.; Ryl, J.; Klimczuk, T.; Zielinska-Jurek, A. Pseudo-superparamagnetic behaviour of barium hexaferrite particles. *RSC Adv.* **2020**, *10*, 18784–18796. [CrossRef]
67. Pullar, R.C. Hexagonal ferrites: A review of the synthesis, properties and applications of hexaferrite ceramics. *Prog. Mater. Sci.* **2012**, *57*, 1191–1334. [CrossRef]
68. Zielińska-Jurek, A.; Bielan, Z.; Wysocka, I.; Strychalska, J.; Janczarek, M.; Klimczuk, T. Magnetic semiconductor photocatalysts for the degradation of recalcitrant chemicals from flow back water. *J. Environ. Manag.* **2017**, *195*, 157–165. [CrossRef]
69. Sutka, A.; Millers, M.; Vanags, M.; Joost, U.; Maiorov, M.; Kisand, V.; Pärna, R.; Juhnevica, I. Comparison of photocatalytic activity for different co-precipitated spinel ferrites. *Res. Chem. Intermed.* **2015**, *41*, 9439–9449. [CrossRef]
70. Dojcinovic, M.P.; Vasiljevic, Z.Z.; Pavlovic, V.P.; Barisic, D.; Pajic, D.; Tadic, N.B.; Nikolic, M.V. Mixed Mg–Co spinel ferrites: Structure, morphology, magnetic and photocatalytic properties. *J. Alloys Compd.* **2021**, *855*, 157429. [CrossRef]
71. Rahmayeni, R.; Oktavia, Y.; Stiadi, Y.; Arief, S.; Zulhadjri, Z. Spinel ferrite of $MnFe_2O_4$ synthesized in Piper betle Linn extract media and its application as photocatalysts and antibacterial. *J. Dispers. Sci. Technol.* **2021**, *42*, 465–474. [CrossRef]
72. Sonu; Sharma, S.; Dutta, V.; Raizada, P.; Hosseini-Bandegharaei, A.; Thakur, V.; Nguyen, V.H.; Vanle, Q.; Singh, P. An overview of heterojunctioned $ZnFe_2O_4$ photocatalyst for enhanced oxidative water purification. *J. Environ. Chem. Eng.* **2021**, *9*, 105812. [CrossRef]
73. Ata, S.; Shaheen, I.; Majid, F.; Bibi, I.; Ijaz-Ul-Mohsin; Jilani, K.; Slimani, Y.; Iqbal, M. Hydrothermal route for the synthesis of manganese ferrite nanoparticles and photocatalytic activity evaluation for the degradation of methylene blue dye. *Z. Phys. Chem.* **2021**, *235*, 1381. [CrossRef]
74. Rashmi, S.K.; Bhojya Naik, H.S.; Jayadevappa, H.; Viswanath, R.; Patil, S.B.; Madhukara Naik, M. Solar light responsive Sm-Zn ferrite nanoparticle as efficient photocatalyst. *Mater. Sci. Eng. B Solid-State Mater. Adv. Technol.* **2017**, *225*, 86–97. [CrossRef]
75. Ajeesha, T.; Ashwini, A.; George, M.; Manikandan, A.; Mary, J.A.; Slimani, Y.; Almessiere, M.A.; Baykal, A. Nickel substituted $MgFe_2O_4$ nanoparticles via co-precipitation method for photocatalytic applications. *Phys. B Condens. Matter* **2021**, *606*, 412660. [CrossRef]
76. George, M.; Ajeesha, T.L.; Manikandan, A.; Anantharaman, A.; Jansi, R.S.; Kumar, E.R.; Slimani, Y.; Almessiere, M.A.; Baykal, A. Evaluation of Cu–$MgFe_2O_4$ spinel nanoparticles for photocatalytic and antimicrobial activates. *J. Phys. Chem. Solids* **2021**, *153*, 110010. [CrossRef]
77. Ghafoor, A.; Bibi, I.; Ata, S.; Majid, F.; Kamal, S.; Rehman, F.; Iqbal, S.; Aamir, M.; Slimani, Y.; Iqbal, M.; et al. Synthesis and characterization of magnetically separable $La_{1-x}Bi_xCr_{1-y}Fe_yO_3$ and photocatalytic activity evaluation under visible light. *Z. Phys. Chem.* **2021**, *235*, 1747. [CrossRef]
78. Bibi, F.; Iqbal, S.; Sabeeh, H.; Saleem, T.; Ahmad, B.; Nadeem, M.; Shakir, I.; Aadil, M. Ambreen kalsoom Evaluation of structural, dielectric, magnetic and photocatalytic properties of Nd and Cu co-doped barium hexaferrite. *Ceram. Int.* **2021**, *47*, 30911–30921. [CrossRef]
79. Ohtani, B.; Prieto-Mahaney, O.O.; Li, D.; Abe, R. What is Degussa (Evonic) P25? Crystalline composition analysis, reconstruction from isolated pure particles and photocatalytic activity test. *J. Photochem. Photobiol. A Chem.* **2010**, *216*, 179–182. [CrossRef]
80. Wang, K.; Wei, Z.; Ohtani, B.; Kowalska, E. Interparticle electron transfer in methanol dehydrogenation on platinum- loaded titania particles prepared from P25. *Catal. Today* **2018**, *303*, 327–333. [CrossRef]
81. Raut, S.S.; Adpa, S.K.; Jambhale, A.; Abhyankar, A.C.; Kulkarni, P.S. Enhanced photocatalytic activity of magnetic $BaFe_{12}O_{19}$ nanoplatelets than TiO_2 with emphasis on reaction kinetics, mechanism, and reusability. *Ind. Eng. Chem. Res.* **2018**, *57*, 16192–16200. [CrossRef]
82. Bavarsiha, F.; Montazeri-Pour, M.; Rajabi, M. Effect of Non-aqueous Media on Nano-crystalline $SrFe_{12}O_{19}$ Particles Produced by Co-precipitation with Metal Chlorides and Evaluation of Their Magnetic and Photocatalytic Properties. *J. Inorg. Organomet. Polym. Mater.* **2020**, *30*, 2386–2396. [CrossRef]
83. Mahdiani, M.; Sobhani, A.; Salavati-Niasari, M. The first synthesis of $CdFe_{12}O_{19}$ nanostructures and nanocomposites and considering of magnetic, optical, electrochemical and photocatalytic properties. *J. Hazard. Mater.* **2019**, *367*, 607–619. [CrossRef]
84. Bibi, I.; Muneer, M.; Iqbal, M.; Alwadai, N.; Almuqrin, A.H.; Altowyan, A.S.; Alshammari, F.H.; Almuslem, A.S.; Slimani, Y. Effect of doping on dielectric and optical properties of barium hexaferrite: Photocatalytic performance under solar light irradiation. *Ceram. Int.* **2021**, *47*, 31518–31526. [CrossRef]
85. Bahnemann, D.; Henglein, A.; Lilie, J.; Spanhel, L. Flash photolysis observation of the absorption spectra of trapped positive holes and electrons in colloidal TiO_2. *J. Phys. Chem.* **1984**, *88*, 709–711. [CrossRef]
86. Pruden, A.L.; Ollis, D.F. Photoassisted heterogeneous catalysis: The degradation of trichloroethylene in water. *J. Catal.* **1983**, *82*, 404–417. [CrossRef]
87. Sclafani, A.; Palmisano, L.; Schiavello, M. Influence of the preparation methods of TiO_2 on the photocatalytic degradation of phenol in aqueous dispersion. *J. Phys. Chem.* **1990**, *94*, 829–832. [CrossRef]
88. Markowska-Szczupak, A.; Endo-Kimura, M.; Paszkiewicz, O.; Kowalska, E. Are titania photocatalysts and titanium implants safe? Review on the toxicity of titanium compounds. *Nanomaterials* **2020**, *10*, 2065. [CrossRef]

89. Ohtani, B.; Osaki, H.; Nishimoto, S.; Kagiya, T. A Novel Photocatalytic Process of Amine N-Alkylation by Platinized Semiconductor Particles Suspended in Alcohols. *J. Am. Chem. Soc.* **1986**, *108*, 308–310. [CrossRef]
90. Zaleska, A. Doped-TiO_2: A Review. *Recent Pat. Eng.* **2008**, *2*, 157–164. [CrossRef]
91. Wang, K.; Bielan, Z.; Endo-Kimura, M.; Janczarek, M.; Zhang, D.; Kowalski, D.; Zielińska-Jurek, A.; Markowska-Szczupak, A.; Ohtani, B.; Kowalska, E. On the mechanism of photocatalytic reactions on Cu_xO@TiO_2 core–shell photocatalysts. *J. Mater. Chem. A* **2021**, *9*, 10135–10145. [CrossRef]
92. Tryba, B.; Tsumura, T.; Janus, M.; Morawski, A.W.; Inagaki, M. Carbon-coated anatase: Adsorption and decomposition of phenol in water. *Appl. Catal. B Environ.* **2004**, *50*, 177–183. [CrossRef]
93. Baran, T.; Macyk, W. Photocatalytic oxidation of volatile pollutants of air driven by visible light. *J. Photochem. Photobiol. A Chem.* **2012**, *241*, 8–12. [CrossRef]
94. Desario, P.A.; Pietron, J.J.; Devantier, D.E.; Brintlinger, T.H.; Stroud, R.M.; Rolison, D.R. Plasmonic enhancement of visible-light water splitting with Au-TiO_2 composite aerogels. *Nanoscale* **2013**, *5*, 8073–8083. [CrossRef]
95. Bielan, Z.; Kowalska, E.; Dudziak, S.; Wang, K.; Ohtani, B.; Zielińska-Jurek, A. Mono- and bimetallic (Pt/Cu) titanium(IV) oxide core–shell photocatalysts with UV/Vis light activity and magnetic separability. *Catal. Today* **2021**, *361*, 198–209. [CrossRef]
96. Mrotek, E.; Dudziak, S.; Malinowska, I.; Pelczarski, D.; Ryżyńska, Z.; Zielińska-Jurek, A. Improved degradation of etodolac in the presence of core-shell $ZnFe_2O_4/SiO_2/TiO_2$ magnetic photocatalyst. *Sci. Total Environ.* **2020**, *724*, 1–12. [CrossRef]
97. Huerta Aguilar, C.A.; Pandiyan, T.; Arenas-Alatorre, J.A.; Singh, N. Oxidation of phenols by TiO_2-Fe_3O_4-M (M=Ag or Au) hybrid composites under visible light. *Sep. Purif. Technol.* **2015**, *149*, 265–278. [CrossRef]
98. Baig, M.M.; Pervaiz, E.; Afzal, M.J. Catalytic activity and kinetic studies of core@shell nanostructure $NiFe_2O_4$@TiO_2 for photocatalytic degradation of methyl orange dye. *J. Chem. Soc. Pak.* **2020**, *42*, 531–541.
99. Ciocarlan, R.G.; Seftel, E.M.; Mertens, M.; Pui, A.; Mazaj, M.; Novak Tusar, N.; Cool, P. Novel magnetic nanocomposites containing quaternary ferrites systems $Co_{0.5}Zn_{0.25}M_{0.25}Fe_2O_4$ (M = Ni, Cu, Mn, Mg) and TiO_2-anatase phase as photocatalysts for wastewater remediation under solar light irradiation. *Mater. Sci. Eng. B Solid-State Mater. Adv. Technol.* **2018**, *230*, 1–7. [CrossRef]
100. Fu, Y.; Chen, Q.; He, M.; Wan, Y.; Sun, X.; Xia, H.; Wang, X. Copper Ferrite-Graphene Hybrid: A Multifunctional Heteroarchitecture for Photocatalysis and Energy Storage. *Ind. Eng. Chem. Res.* **2012**, *51*, 11700–11709. [CrossRef]
101. Jia, Y.; Liu, J.; Cha, S.; Choi, S.; Chang, Y.C.; Liu, C. Magnetically separable Au-TiO_2/nanocube $ZnFe_2O_4$ composite for chlortetracycline removal in wastewater under visible light. *J. Ind. Eng. Chem.* **2017**, *47*, 303–314. [CrossRef]
102. Zielińska-Jurek, A.; Bielan, Z.; Dudziak, S.; Wolak, I.; Sobczak, Z.; Klimczuk, T.; Nowaczyk, G.; Hupka, J. Design and application of magnetic photocatalysts for water treatment. The effect of particle charge on surface functionality. *Catalysts* **2017**, *7*, 360. [CrossRef]
103. Sibi, M.G.; Verma, D.; Kim, J. Magnetic core–shell nanocatalysts: Promising versatile catalysts for organic and photocatalytic reactions. *Catal. Rev.* **2019**, *62*, 163–311. [CrossRef]
104. Zhang, Q.; Meng, G.; Wu, J.; Li, D.; Liu, Z. Study on enhanced photocatalytic activity of magnetically recoverable Fe_3O_4@C@TiO_2 nanocomposites with core—Shell nanostructure. *Opt. Mater.* **2015**, *46*, 52–58. [CrossRef]
105. Fu, W.; Yang, H.; Li, M.; Chang, L.; Yu, Q.; Xu, J.; Zou, G. Preparation and photocatalytic characteristics of core-shell structure $TiO_2/BaFe_{12}O_{19}$ nanoparticles. *Mater. Lett.* **2006**, *60*, 2723–2727. [CrossRef]
106. Lee, S.W.; Drwiega, J.; Wu, C.Y.; Mazyck, D.; Sigmund, W.M. Anatase TiO_2 Nanoparticle Coating on Barium Ferrite Using Titanium Bis-Ammonium Lactato Dihydroxide and Its Use as a Magnetic Photocatalyst. *Chem. Mater.* **2004**, *16*, 1160–1164. [CrossRef]
107. Xie, T.; Xu, L.; Liu, C.; Zhang, X. A novel magnetic heterojunction photocatalyst $TiO_2/SrFe_{12}O_{19}$: Synthesis strategy, photocatalytic activity, and unprecedented migration mechanism of photoexcited charge carrier. *Mater. Technol.* **2018**, *33*, 582–591. [CrossRef]
108. Bavarsiha, F.; Rajabi, M.; Montazeri-Pour, M. Synthesis of $SrFe_{12}O_{19}/SiO_2/TiO_2$ composites with core/shell/shell nano-structure and evaluation of their photo-catalytic efficiency for degradation of methylene blue. *J. Mater. Sci. Mater. Electron.* **2017**, *29*, 1877–1887. [CrossRef]
109. Lahijani, B.; Hedayati, K.; Goodarzi, M. Magnetic $PbFe_{12}O_{19}$-TiO_2 nanocomposites and their photocatalytic performance in the removal of toxic pollutants. *Main Gr. Met. Chem.* **2018**, *41*, 53–62. [CrossRef]
110. Kubiak, A.; Bielan, Z.; Bartkowiak, A.; Gabała, E.; Piasecki, A.; Zalas, M.; Zielińska-Jurek, A.; Janczarek, M.; Siwińska-Ciesielczyk, K.; Jesionowski, T. Synthesis of titanium dioxide via surfactant-assisted microwave method for photocatalytic and dye-sensitized solar cells applications. *Catalysts* **2020**, *10*, 586. [CrossRef]
111. Dudziak, S.; Kowalkińska, M.; Karczewski, J.; Pisarek, M.; Siuzdak, K.; Kubiak, A.; Siwińska-Ciesielczyk, K.; Zielińska-Jurek, A. Solvothermal growth of {0 0 1} exposed anatase nanosheets and their ability to mineralize organic pollutants. The effect of alcohol type and content on the nucleation and growth of TiO_2 nanostructures. *Appl. Surf. Sci.* **2021**, *563*, 150360. [CrossRef]
112. Kubiak, A.; Żółtowska, S.; Gabała, E.; Szybowicz, M.; Siwińska-Ciesielczyk, K.; Jesionowski, T. Controlled microwave-assisted and pH-affected growth of ZnO structures and their photocatalytic performance. *Powder Technol.* **2021**, *386*, 221–235. [CrossRef]
113. Kubiak, A.; Bielan, Z.; Kubacka, M.; Gabała, E.; Zgoła-Grześkowiak, A.; Janczarek, M.; Zalas, M.; Zielińska-Jurek, A.; Siwińska-Ciesielczyk, K.; Jesionowski, T. Microwave-assisted synthesis of a TiO_2-CuO heterojunction with enhanced photocatalytic activity against tetracycline. *Appl. Surf. Sci.* **2020**, *520*, 146344. [CrossRef]

114. Palanisamy, G.; Bhuvaneswari, K.; Bharathi, G.; Pazhanivel, T.; Grace, A.N.; Pasha, S.K.K. Construction of magnetically recoverable ZnS–WO_3–$CoFe_2O_4$ nanohybrid enriched photocatalyst for the degradation of MB dye under visible light irradiation. *Chemosphere* **2021**, *273*, 129687. [CrossRef]
115. Abroshan, E.; Farhadi, S.; Zabardasti, A. Novel magnetically separable Ag_3PO_4/$MnFe_2O_4$ nanocomposite and its high photocatalytic degradation performance for organic dyes under solar-light irradiation. *Sol. Energy Mater. Sol. Cells* **2018**, *178*, 154–163. [CrossRef]
116. Javed, H.; Rehman, A.; Mussadiq, S.; Shahid, M.; Khan, M.A.; Shakir, I.; Agboola, P.O.; Aboud, M.F.A.; Warsi, M.F. Reduced graphene oxide-spinel ferrite nano-hybrids as magnetically separable and recyclable visible light driven photocatalyst. *Synth. Met.* **2019**, *254*, 1–9. [CrossRef]
117. Jun, B.M.; Elanchezhiyan, S.S.; Yoon, Y.; Wang, D.; Kim, S.; Muthu Prabhu, S.; Park, C.M. Accelerated photocatalytic degradation of organic pollutants over carbonate-rich lanthanum-substituted zinc spinel ferrite assembled reduced graphene oxide by ultraviolet (UV)-activated persulfate. *Chem. Eng. J.* **2020**, *393*, 124733. [CrossRef]
118. Dudziak, S.; Bielan, Z.; Kubica, P.; Zielińska-Jurek, A. Optimization of carbamazepine photodegradation on defective TiO_2-based magnetic photocatalyst. *J. Environ. Chem. Eng.* **2021**, *9*, 105782. [CrossRef]
119. Safizade, B.; Masoudpanah, S.M.; Hasheminiasari, M.; Ghasemi, A. Photocatalytic activity of $BiFeO_3$/$ZnFe_2O_4$ nanocomposites under visible light irradiation. *RSC Adv.* **2018**, *8*, 6988–6995. [CrossRef]
120. Zhang, R.; Han, Q.; Li, Y.; Zhang, T.; Liu, Y.; Zeng, K.; Zhao, C. Solvothermal synthesis of a peony flower-like dual Z-scheme PANI/BiOBr/$ZnFe_2O_4$ photocatalyst with excellent photocatalytic redox activity for organic pollutant under visible-light. *Sep. Purif. Technol.* **2020**, *234*, 116098. [CrossRef]
121. Mahdiani, M.; Sobhani, A.; Salavati-Niasari, M. Enhancement of magnetic, electrochemical and photocatalytic properties of lead hexaferrites with coating graphene and CNT: Sol-gel auto-combustion synthesis by valine. *Sep. Purif. Technol.* **2017**, *185*, 140–148. [CrossRef]
122. Ismail, A.A.; Al-Hajji, L.A.; Albukhari, S.M.; Mahmoud, M.H.H. Promoting the solar-light-driven Mesoporous $BaFe_{12}O_{19}$/g-C_3N_4 Photocatalysts for Photoreduction and Removal of Hg(II) Ions. *Surf. Interfaces* **2021**, *26*, 101387. [CrossRef]
123. Wang, H.; Xu, Y.; Jing, L.; Huang, S.; Zhao, Y.; He, M.; Xu, H.; Li, H. Novel magnetic $BaFe_{12}O_{19}$/g-C_3N_4 composites with enhanced thermocatalytic and photo-Fenton activity under visible-light. *J. Alloys Compd.* **2017**, *710*, 510–518. [CrossRef]
124. Aziz, A.; Yau, Y.H.; Puma, G.L.; Fischer, C.; Ibrahim, S.; Pichiah, S. Highly efficient magnetically separable TiO_2-graphene oxide supported $SrFe_{12}O_{19}$ for direct sunlight-driven photoactivity. *Chem. Eng. J.* **2014**, *235*, 264–274. [CrossRef]
125. Xie, T.; Xu, L.; Liu, C.; Wang, Y. Magnetic composite $ZnFe_2O_4$/$SrFe_{12}O_{19}$: Preparation, characterization, and photocatalytic activity under visible light. *Appl. Surf. Sci.* **2013**, *273*, 684–691. [CrossRef]
126. Sobhani-Nasab, A.; Behpour, M.; Rahimi-Nasrabadi, M.; Ahmadi, F.; Pourmasoud, S. New method for synthesis of $BaFe_{12}O_{19}$/$Sm_2Ti_2O_7$ and $BaFe_{12}O_{19}$/$Sm_2Ti_2O_7$/Ag nano-hybrid and investigation of optical and photocatalytic properties. *J. Mater. Sci. Mater. Electron.* **2019**, *30*, 5854–5865. [CrossRef]
127. Kraeutler, B.; Bard, A.J. Heterogeneous Photocatalytic Preparation of Supported Catalysts. Photodeposition of Platinum on TiO_2 Powder and Other Substrates. *J. Am. Chem. Soc.* **1978**, *100*, 4317–4318. [CrossRef]
128. Ohtani, B.; Kakimoto, M.; Nishimoto, S.; Kagiya, T. Photocatalytic reaction of neat alcohols by metal-loaded titanium(IV) oxide particles. *J. Photochem. Photobiol. A Chem.* **1993**, *70*, 265–272. [CrossRef]
129. Ohtani, B.; Nishimoto, S. Effect of surface adsorptions of aliphatic alcohols and silver ion on the photocatalytic activity of TiO_2 suspended in aqueous solutions. *J. Phys. Chem.* **1993**, *97*, 920–926. [CrossRef]
130. Kowalska, E.; Remita, H.; Colbeau-Justin, C.; Hupka, J.; Belloni, J. Modification of Titanium Dioxide with Platinum Ions and Clusters: Application in Photocatalysis. *J. Phys. Chem. C* **2008**, *112*, 1124–1131. [CrossRef]
131. Xie, T.; Hu, J.; Yang, J.; Liu, C.; Xu, L.; Wang, J.; Peng, Y.; Liu, S.; Yin, X.; Lu, Y. Visible-light-driven photocatalytic activity of magnetic BiOBr/$SrFe_{12}O_{19}$ nanosheets. *Nanomaterials* **2019**, *9*, 735. [CrossRef]
132. Xu, Y.; Ge, F.; Xie, M.; Huang, S.; Qian, J.; Wang, H.; He, M.; Xu, H.; Li, H. Fabrication of magnetic $BaFe_{12}O_{19}$/Ag_3PO_4 composites with an: In situ photo-Fenton-like reaction for enhancing reactive oxygen species under visible light irradiation. *Catal. Sci. Technol.* **2019**, *9*, 2563–2570. [CrossRef]
133. Wang, C.; Zhang, X.; Liu, Y. Promotion of multi-electron transfer for enhanced photocatalysis: A review focused on oxygen reduction reaction. *Appl. Surf. Sci.* **2015**, *358*, 28–45. [CrossRef]
134. Chen, X.; Dai, Y.; Wang, X. Methods and mechanism for improvement of photocatalytic activity and stability of Ag_3PO_4: A review. *J. Alloys Compd.* **2015**, *649*, 910–932. [CrossRef]
135. da S. Pereira, W.; Gozzo, C.B.; Longo, E.; Leite, E.R.; Sczancoski, J.C. Investigation on the photocatalytic performance of $Ag_4P_2O_7$ microcrystals for the degradation of organic pollutants. *Appl. Surf. Sci.* **2019**, *493*, 1195–1204. [CrossRef]
136. Xie, M.; Wang, D.; Jing, L.; Wei, W.; Xu, Y.; Xu, H.; Li, H.; Xie, J. Preparation of magnetically recoverable and Z-scheme $BaFe_{12}O_{19}$/AgBr composite for degradation of 2-Mercaptobenzothiazole and Methyl orange under visible light. *Appl. Surf. Sci.* **2020**, *521*, 146343. [CrossRef]
137. Chen, S.; Di, Y.; Li, H.; Wang, M.; Jia, B.; Xu, R.; Liu, X. Efficient photocatalytic dye degradation by flowerlike MoS_2/$SrFe_{12}O_{19}$ heterojunction under visible light. *Appl. Surf. Sci.* **2021**, *559*, 149855. [CrossRef]
138. Xie, T.; Liu, C.; Xu, L.; Yang, J.; Zhou, W. Novel heterojunction Bi_2O_3/$SrFe_{12}O_{19}$ magnetic photocatalyst with highly enhanced photocatalytic activity. *J. Phys. Chem. C* **2013**, *117*, 24601–24610. [CrossRef]

139. Wang, H.; Xu, L.; Liu, C.; Jiang, Z.; Feng, Q.; Wu, T.; Wang, R. A novel magnetic photocatalyst $Bi_3O_4Cl/SrFe_{12}O_{19}$: Fabrication, characterization and its photocatalytic activity. *Ceram. Int.* **2020**, *46*, 460–467. [CrossRef]
140. Wang, H.; Xu, L.; Wu, X.; Zhang, M. Eco-friendly synthesis of a novel magnetic $Bi_4O_5Br_2/SrFe_{12}O_{19}$ nanocomposite with excellent photocatalytic activity and recyclable performance. *Ceram. Int.* **2021**, *47*, 8300–8307. [CrossRef]
141. Wang, S.; Gao, H.; Fang, L.; Hu, Q.; Sun, G.; Chen, X.; Yu, C.; Tang, S.; Yu, X.; Zhao, X.; et al. Synthesis of novel CQDs/CeO_2/$SrFe_{12}O_{19}$ magnetic separation photocatalysts and synergic adsorption-photocatalytic degradation effect for methylene blue dye removal. *Chem. Eng. J. Adv.* **2021**, *6*, 100089. [CrossRef]
142. Mesdaghi, S.; Yousefi, M.; Hossaini sadr, M.; Mahdavian, A. The effect of PANI and MWCNT on magnetic and photocatalytic properties of substituted barium hexaferrite nanocomposites. *Mater. Chem. Phys.* **2019**, *236*, 121786. [CrossRef]
143. Khandani, M.; Yousefi, M.; Afghahi, S.S.S.; Amini, M.M.; Bikhof Torbati, M. $Sr(CeNd)_xFe_{12-2x}O_{19}$/polythiophene nano-particles: Structral investigation, magnetic properties and photocatalyic activity. *Inorg. Chem. Commun.* **2020**, *121*, 108214. [CrossRef]
144. Kowalkińska, M.; Dudziak, S.; Karczewski, J.; Ryl, J.; Trykowski, G.; Zielińska-Jurek, A. Facet effect of TiO_2 nanostructures from $TiOF_2$ and their photocatalytic activity. *Chem. Eng. J.* **2021**, *404*, 126493. [CrossRef]